# Surgical Removal of Visceral Adipose Tissue has Therapeutic Benefit in Male $APP^{NL-F}$ Mice

Samuel A. McFadden[1†], Yimin Fang[1†], Kathleen Quinn[1], Mackenzie R. Peck[1], Jenelle E. Chapman[1], Tiarra Hill[1], Andrzej Bartke[2,3], Erin R. Hascup[1,4], Kevin N. Hascup[1,3,4*]

[1]Dale and Deborah Smith Center for Alzheimer's Research and Treatment, [2]Internal Medicine, [3]Medical Microbiology, Immunology and Cell Biology, and [4]Pharmacology, at Southern Illinois University School of Medicine, Springfield, IL, USA

[†]These authors contributed equally to this work and share first authorship.

*Corresponding Author: Kevin N. Hascup, Dale and Deborah Smith Center for Alzheimer's Research and Treatment, Southern Illinois University School of Medicine, P.O. Box 19628, Springfield, IL 62794-9628, USA Tel: 217-545-6994, Email: khascup49@siumed.edu

Keywords: Alzheimer's disease, lipectomy, white adipose tissue, cell senescence, glucose and lipid metabolism, inflammation, visfatin

Manuscript Length: 5,557 Words

Figures: 7

Tables: 2

**Abstract**

Purpose: Visceral white adipose tissue (vWAT) accumulation causes systemic inflammation, insulin resistance, metabolic syndrome, and senescent cell accumulation that are risk factors for Alzheimer's disease (AD). Visceral fat removal (VFR) improves metabolism and reduces pro-inflammatory cytokines. We hypothesized that VFR removal in AD mice would improve metabolism and cognition.

Methods: Male and female $APP^{NL-F}$ mice underwent sham or vWAT surgical resection (periovarian or epididymal and perirenal) at 4 (pre-symptomatic) and 16 (symptomatic) months of age to understand interventional and therapeutic effects, respectively. At 18 months of age, glucose metabolism and novel object recognition (NOR) memory were assayed followed by assessment of body composition and tissue-specific markers of metabolism, cell senescence, inflammation, or amyloid accumulation.

Results: Male and female $APP^{NL-F}$ mice showed distinct VFR responses. In pre-symptomatic males, increased vWAT lipolysis and hepatic lipogenesis led to ectopic liver lipid accumulation, with reduced adiponectin and leptin, elevated visfatin, and impaired glucose metabolism. Symptomatic males showed reduced vWAT lipogenesis, enhanced hepatic lipolysis, glycolysis, and glycogenesis, lowering liver lipids and improving insulin sensitivity. Only symptomatic males improved NOR, linked to elevated hippocampal learning and memory markers. Female vWAT reaccumulation was due to increased lipogenesis and lower lipolysis. Pre-symptomatic females had lower hepatic lipogenesis, while glycolysis and glycogenesis declined with disease progression. Hippocampal senescence and inflammation were elevated early in the disease that persisted symptomatically.

Conclusions: Sex-specific differences in glucose and lipid metabolism and lipid accumulation underlie the divergent responses to VFR in $APP^{NL-F}$ mice, with symptomatic males showing the only beneficial outcomes in metabolism and cognition.

## Graphical Abstract

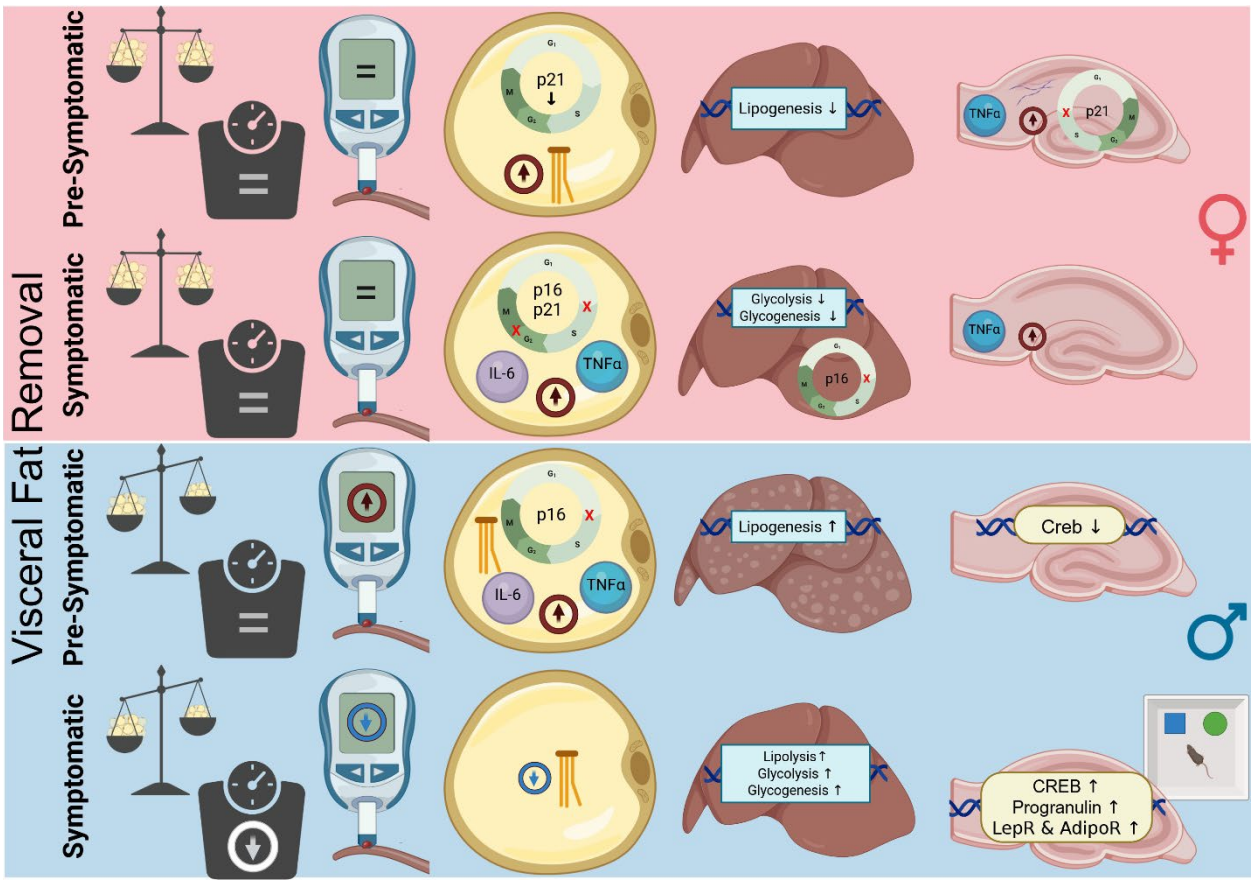


Male and female APP$^{NL-F}$ mice exhibited distinct VFR responses to AD progression. In males, early disease stages were marked by vWAT lipolysis and hepatic lipid accumulation with metabolic dysfunction, while symptomatic stages showed a metabolic shift that improved insulin sensitivity and NOR performance. In contrast, females displayed progressive vWAT reaccumulation, reduced hepatic metabolism, and persistent hippocampal senescence and inflammation from early stages onward.

50 **Introduction**

51 AD is a progressive, neurodegenerative disorder, and the most prevalent form of dementia. AD
52 is historically characterized by senile plaques composed of aggregated amyloid beta (Aβ) and
53 neurofibrillary tangles formed from hyperphosphorylated tau protein. However, AD is a
54 multifactorial disorder characterized not only by aberrant protein aggregation, but also by
55 mitochondrial dysfunction, oxidative stress, cellular senescence, and chronic inflammation - all
56 of which contribute to disease progression (Breijyeh and Karaman, 2020). The deleterious
57 cascade underlying AD progression is hypothesized to begin in midlife and is not isolated to the
58 CNS. Peripheral organs, such as vWAT, regulate brain function through hormone secretion as
59 well as glucose and lipid metabolism (Gustafson, 2012, Dove et al., 2021). Accumulation of
60 vWAT in midlife is a predictor for future development of AD (Huang et al., 2022).

61 Adipose tissue regulates many aspects of whole-body physiology, including food intake,
62 maintenance of energy levels, insulin sensitivity, body temperature, and immune responses
63 (Sakers et al., 2022). Adipose tissue is located under the skin (subcutaneous; SubQ), between
64 and around organs (vWAT), interscapular brown adipose tissue (BAT), in bone marrow, and in
65 mammary glands (Wong Zhang et al., 2023). Beyond total adipose tissue mass, the distribution
66 of fat depots is a stronger predictor of obesity-related disease risk and associated complications
67 (Chusyd et al., 2016). Excess vWAT accumulation causes systemic inflammation, insulin
68 resistance, reduced cerebral blood flow, and metabolic syndrome, which contributes to brain
69 volume shrinkage and cognitive decline (Richard et al., 2000, Wong Zhang et al., 2023,
70 Baglietto-Vargas et al., 2016, Biessels and Despa, 2018, Dove et al., 2021, Nguyen et al.,
71 2014).

72 The link between systemic inflammation with vWAT and metabolic dysfunction has been
73 reported in diabetic fatty rodents and in aged rats (Borst et al., 2005, Gabriely et al., 2002,
74 Pitombo et al., 2006). In humans, vWAT is a stronger predictor of age-related cognitive

impairment than body mass index (Whitmer et al., 2008, Elias et al., 2005, Kamogawa et al., 2010). A cross-sectional study also showed that vWAT dysfunction and inflammatory status in obesity, is associated with increased cerebral Aβ burden in midlife (Kim et al., 2022). Transplantation of vWAT from obese mice led to impaired cognition in lean wild-type recipient mice mediated by NLRP3/IL-1β signaling (Guo et al., 2020). The effects of VFR are broadly similar to observations in calorie restricted rodents (Masternak et al, 2012). VFR prevented obesity-induced insulin resistance, hyperinsulinemia, and decreased plasma pro-inflammatory cytokine levels (Borst et al., 2005, Gabriely et al., 2002, Pitombo et al., 2006), which improved glucose metabolism (Barzilai et al., 1999, Foster et al., 2011, Franczyk et al., 2021). Aging also increases vWAT senescent cell burden leading to a chronic pro-inflammatory state (Tchkonia et al., 2010). Reduction of senescent cells in vWAT improves metabolic and cognitive performance in normal aging (Fang et al., 2023) and AD mice (Fang et al, 2025).

Considering the contribution of vWAT accumulation on cognitive decline and AD progression, we hypothesized that surgical resection of this adipose depot would improve the metabolic profile and reduce cognitive impairments in the $APP^{NL-F}$ AD mouse model. $APP^{NL-F}$ mice contain the human Aβ isoform of the Swedish (KM670/671NL) and Iberian (I716F) mutations knocked into the *App* locus leading to upregulation of $A\beta_{42}$ without overexpression of APP (Saito et al., 2014, Benitez et al., 2021). Plaque accumulation begins at ~6 months of age while cognitive impairments occur between 12-18 months of age. Our prior research indicates that both sexes of $APP^{NL-F}$ mice have increased markers of senescent cell ($p16^{Ink4\alpha}$ and $p21^{Cip1}$) and senescence-associated secretory phenotype (SASP; IL-6, TNFα, MIP1α) in vWAT by 4 months of age (Fang et al., 2025), which may account for their reduced glucose tolerance (Abi-Ghanem et al., 2025). Besides metabolic dysfunction, senescent adipocytes also contribute to chronic systemic inflammation which diminishes cognitive reserve, promotes the accumulation of misfolded proteins, and accelerates AD progression (Huang et al, 2022).

100 To test our hypothesis, we surgically resected vWAT (periovarian or epididymal and perirenal,
101 hereafter perigonadal) from male and female $APP^{NL-F}$ mice at either 4 or 16 months of age.
102 These time points allowed us to examine the effects of VFR for pre-symptomatic intervention (4
103 months) or symptomatic therapy (16 months). All metabolic and cognitive assays were
104 conducted at 18 months of age. Our results indicate that VFR effects were disease stage- and
105 sex-dependent with metabolic and cognitive benefits observed in symptomatic male $APP^{NL-F}$
106 mice.

107 **Material and Methods**

108 Chemicals

109 All chemicals were stored according to manufacturer recommendations unless stated otherwise.
110 The Phosphovanilin reagent for lipid determination was prepared by using 6 milligrams of
111 vanillin (Fisher Scientific Cat # AC140821000) dissolved in 100 mL of 37°C $H_2O$ and further
112 diluted to 500 mL with 85% phosphoric acid.

113 Animals

114 Founder $APP^{NL-F}$ mice on a C57BL/6 background (RRID: IMSR_RBRC06343) were obtained
115 from Riken (Japan). C57BL/6 (RRID:IMSR_JAX:000664) mice were originally obtained from The
116 Jackson Laboratory (Bar Harbor, ME) and used to maintain the genetic background of the
117 breeding colonies. At weaning, pups were randomly assigned to mixed-litter cages and group-
118 housed with mice of the same sex and genotype to control for litter size, maternal care, and
119 other potential litter-specific variables. Protocols for animal use were approved by the
120 Institutional Animal Care and Use Committee at Southern Illinois University School of Medicine
121 (Protocol number: 2025-055), which is accredited by the Association for Assessment and
122 Accreditation of Laboratory Animal Care. All studies were conducted in accordance with the
123 United States Public Health Service's Policy on Humane Care and Use of Laboratory Animals.
124 Mice were group housed on a 12:12 h light-dark cycle, with food (Chow 5001 with 23.4%
125 protein, 5% fat, and 5.8% crude fiber; LabDiet PMI Feeds) and water available *ad libitum*.
126 Genotypes were confirmed by collecting a 5 mm tail tip for DNA analysis by TransnetYX, Inc
127 (Cordova, TN). The number of mice in each cohort used for the study are shown in Table 1.

128 VFR Surgery

129 4 and 16-month-old male and female $APP^{NL-F}$ mice were randomized into two groups – VFR
130 (perigonadal) and sham-operated. Mice were isoflurane anesthetized, abdominal fur shaved,

131 and betadine scrubbed over the incision site. An ~1.5 cm vertical midline incision along the
132 lower abdomen in males or ventral incisions on either lateral abdominal side in females were
133 made to access epidydimal adipose depots. The perinephric adipose depots were removed by
134 flank incisions. Adipose depots were removed by blunt dissection. Mice that underwent the
135 sham operation had their vWAT mobilized, but not removed. Absorbable sutures were used to
136 close the body cavity while wound clips were used on the skin. Tylenol (1 mg/mL) was
137 administered in the drinking water from one day pre- to 3 days post-surgery. Table 1 shows the
138 number of mice that were euthanized two weeks or less post-surgery for each group.

139 Glucose tolerance test (GTT) and insulin tolerance test (ITT)

140 Glucose metabolism was assessed via GTT and ITT when mice reached 18 months of age (14
141 or 2 months post VFR surgery) as previously described (Fang et al., 2023). Fifteen-hour-fasted
142 mice underwent GTT by intraperitoneal (ip) injection with 2.0 g glucose per kg of body weight
143 (BW). Blood glucose levels were measured at 0, 15, 30, 45, 60, and 120 min with a PRESTO
144 glucometer (AgaMatrix). For ITT, mice were injected ip with 1 IU insulin glargine (Sanofi-
145 Aventis) per kg of BW. Blood glucose levels were measured at 0, 15, 30, 45, 60, and 120 min.

146 NOR task

147 Object recognition memory was assessed when mice reached ~19 months of age (15 or 3
148 months post VFR surgery). The NOR was used to evaluate memory retention based on the
149 premise that mice spend more time exploring a novel object rather than a familiar object if the
150 animal remembers the familiar object. Mice were habituated in the open field chamber for 30
151 min on the first day. 24 hours after, the mouse was returned to the chamber and presented with
152 two similar objects for 5 min. A 24 hr inter-session-interval was used between introduction and
153 retention phases to promote long-term memory retrieval. During the retention phase one of the
154 familiar objects was replaced with a novel object and the mouse was given 5 minutes of

155 exploration. The ANY-maze video tracking system (Stoelting Co., Wood Dale, IL) was used to
156 record mouse navigation during the familiarization and retention phases and used to calculate
157 the retention index and novelty preference.

158 Body composition and tissue procurement

159 At 19 months of age, BW was recorded and unfasted mice were anesthetized using isoflurane.
160 A cardiac puncture was used to collect the plasma. The blood was mixed with EDTA, followed
161 by centrifugation at 10,000 g for 15 min at 4°C for plasma collection. Immediately following
162 cardiac puncture, mice were decapitated and the peripheral tissues (liver, pancreas,
163 perigonadal and SubQ, WAT, and BAT were weighed to calculate their contribution to total BW.
164 Tissue was immediately flash frozen and stored at -80˚C until processing as previously
165 described (Fang et al., 2023).

166 vWAT Histomorphology and Quantification

167 Frozen vWAT was transferred to ice cold 4% paraformaldehyde in phosphate buffer (pH 7.2)
168 and fixed at 4˚C for 72 hrs. Tissue was then cryoprotected in 30% sucrose in phosphate buffer
169 (pH 7.2) and stored at 4˚C for a minimum of 24 hrs. Following fixation, samples were embedded
170 in optimal cutting temperature compound (Fisher Scientific Cat #23-730-571) using 15 mm
171 cryomolds (Fisher Scientific Cat #22-363-553) on dry ice. Sections (10 µm) were cut using a
172 Leica CM1950 cryostat (chamber -30˚C; specimen holder -40˚C) and mounted on gelatin-
173 coated, charged glass slides (Fisher Scientific, Cat #12-550-15). Slides were air-dried at room
174 temperature (~25˚C) for at least 15 minutes and stored at 4˚C until staining. Slide-mounted
175 vWAT sections were stained according to the manufacturer's instructions using a commercial
176 hematoxylin and eosin (H&E) staining kit (Abcam Cat # ab245880). Following staining and
177 dehydration, sections were cleared with xylene substitute (Fisher Scientific Cat #9990505) and
178 coverslipped with Permount mounting medium (Fisher Scientific Cat # SP15-100). Brightfield

179 images were acquired at 40x magnification using a BZ-X810 All-in-One Flourescence
180 microscope (Keyence Corp). For each sample, four fields of view from four separate section
181 were imaged (16 images per sample). Adipocyte number and interior area ($\mu m^2$) were quantified
182 for each field using the Hybrid Cell Count software (Keyence Corp.). Measurements were
183 averaged across fields and sections to generate a single mean adipocyte count and sample
184 area per mouse.

185 Total Liver Lipid Quantification

186 A modified micro-scale colorimetric sulfo-phospho-vanillin method was used to measure total
187 liver lipids (Tran et al., 2019). Approximately 50 mg of liver tissue was homogenized in 1000 µL
188 of chloroform/methanol (2:1) followed by addition of 500 µL of saline. The mixture was vortexed
189 then centrifuged at 10,000 rpm for 5 minutes. The chloroform layer was separated and
190 evaporated at 90°C for ~20 min, then incubated at 90°C with 200 µL of 98% sulfuric acid for 20
191 min. After adding 750 µL of vanillin–phosphoric acid reagent, samples were incubated at 37˚C
192 for 15 min, cooled to 25˚C, and 200 µL was transferred to a 96-well microplate. Absorbance was
193 measured at 530 nm, and lipid content was normalized to tissue weight.

194 Assessment of blood chemistry

195 Per the manufacturer's protocol, adiponectin or leptin was measured with respective ELISA kits
196 from Crystal Chem (Elk Grove Village, IL; Cat# 80569, 90030). Visfatin was measured by an
197 ELISA kit from Mybiosource (San Diego, CA; Cat# MBS760980).

198 RT–PCR

199 mRNA expression was analyzed by quantitative RT–PCR as previously described (Fang et al.,
200 2020) using Bio-Rad cDNA synthesis kits (Cat # 1708897 and 1708891) and SYBR green mix
201 (Cat # 1725121) and the QuantStudio 3 Real-Time PCR (Thermo Fisher Scientific). RNA was
202 extracted using a RNeasy mini kit or RNeasy Lipid Tissue Mini Kit (Qiagen) following the

203 manufacturer's instructions. Relative expression was calculated as previously described
204 (Masternak et al., 2012) and primers were purchased from Integrated DNA Technologies. A list
205 of forward and reverse primers used in this study is shown in Table 2.

206 Soluble $A\beta_{42}$ Quantification

207 The hippocampus from one hemisphere was dissected and stored at -80°C until tissue
208 processing. Soluble $A\beta_{42}$ concentrations were determined using the Human / Rat β amyloid
209 ELISA kits (WAKO Chemicals; Cat: 290-62601) according to the manufacturer recommended
210 protocols.

211 Statistical analysis

212 Statistical analyses were conducted to determine differences between age- and sex-matched
213 sham and VFR groups. Statistical tests and post hoc analyses are indicated in each Figure
214 legend. A Grubb's test was used to identify outliers. Significance was defined as $p < 0.05$ and
215 investigatory as $p < 0.10$. Data are presented as mean ± SEM. All statistical analyses and
216 graphs were completed using Prism 10 (GraphPad Inc, La Jolla, CA, USA).

217 **Results**

218 <u>VFR at the symptomatic time point improved object recognition memory in male APP$^{NL-F}$ mice.</u>

219 To explore whether VFR could improve object recognition memory in APP$^{NL-F}$ mice, surgery was
220 performed at a pre-symptomatic stage (4 months of age, prior to detectable plaque
221 accumulation and cognitive decline) or a symptomatic stage (16 months of age, during
222 advanced pathology and functional decline). Both male and female APP$^{NL-F}$ cohorts were
223 included to assess sex-specific effects of VFR. Object recognition memory was assayed at 18
224 months of age via the NOR task. Only male APP$^{NL-F}$ mice that underwent VFR at the
225 symptomatic time point had improved recognition memory as indicated by increased retention
226 index (Fig. 1A) and novelty preference (Fig. 1B) compared to the age- and sex-matched sham
227 surgery controls. VFR surgery performed at the pre-symptomatic time point in male, or either
228 time point of female APP$^{NL-F}$, had no effect on object recognition memory (Fig 1A-B).

229 <u>VFR resulted in changes to BW and composition in an age- and sex-dependent manner.</u>

230 To assess physiological changes caused by VFR, we examined body composition at ~19
231 months of age upon euthanasia. VFR decreased BW at the symptomatic stage in male APP$^{NL-F}$
232 mice compared to the sham group (Fig 1C). No differences were observed in the other VFR
233 groups. The body composition analyses indicated that after VFR, vWAT accumulated in all
234 ages and sexes but at different percentages. After VFR, APP$^{NL-F}$ mice had vWAT
235 reaccumulation occurring in 92% and 100% of mice in the pre-symptomatic and symptomatic
236 cohorts, respectively (Fig. 1D). In contrast, ~50% of the male mice undergoing VFR surgery at
237 either age observed vWAT reaccumulation (Fig. 1D). This difference in vWAT was the major
238 contributor to the observed changes of total percent adipose mass when including SubQ,
239 interscapular BAT, and vWAT (Fig. 1E). In summary, the BW of symptomatic male APP$^{NL-F}$ mice
240 after VFR was reduced mainly due to less vWAT reaccumulation.

241 Reaccumulated vWAT in pre-symptomatic male $APP^{NL-F}$ mice had increased adipocyte number
242 and smaller size.

243 H&E staining was used to examine if reaccumulated vWAT had morphological differences.
244 Representative 40x images of pre-symptomatic male sham and VFR $APP^{NL-F}$ cohorts are shown
245 in Fig. 1F. Reaccumulated vWAT following VFR in this cohort exhibited adipocyte hyperplasia
246 characterized by a reduced mean internal diameter (Fig. 1G), and may account for the observed
247 decrease in vWAT mass (Fig. 1E). No differences were observed in the other VFR treated
248 groups compared to sham littermates.

249 VFR during the pre-symptomatic time point in male $APP^{NL-F}$ mice caused ectopic liver lipid
250 deposition via increased de novo lipogenesis.

251 Although vWAT reaccumulated similarly after VFR regardless of disease stage in male $APP^{NL-F}$
252 mice, BW at the time of euthanasia was comparable between pre-symptomatic males after VFR
253 and their sham controls. Body composition changes without effects on BW are known to happen
254 with aging (St-Onge and Gallagher, 2010). We sought to identify tissue composition changes
255 that caused the increased BW despite reduced adiposity in the pre-symptomatic male mice after
256 VFR. Lipodystrophy leads to the excessive deposition of lipids in other organs, such as the liver
257 or muscle, contributing to insulin resistance (Petersen and Shulman, 2018). To test whether the
258 liver had more ectopic lipid deposition, the percentage of total liver lipids was measured. Pre-
259 symptomatic male $APP^{NL-F}$ mice had a higher percentage of liver lipids after VFR compared with
260 sham controls (Fig 2A). In symptomatic $APP^{NL-F}$ male mice, VFR reduced total liver lipids
261 compared with sham surgery controls while no differences were observed in females at either
262 disease stage.

263 Liver gene expression showed that key *de novo* lipogenesis genes including acetyl-coenzyme A
264 carboxylase (ACC), fatty acid synthase (FAS), stearoyl-CoA desaturase 1 (SCD1), elongation of

265 long-chain fatty acids family member 6 (Elovl6), sterol regulatory element-binding protein-1
266 (SREBP1) were increased after VFR in pre-symptomatic male $APP^{NL-F}$ mice compared with
267 sham controls (Fig 2B). In pre-symptomatic female $APP^{NL-F}$ mice, expression of these same
268 genes (except for ACC) were decreased after VFR. Interestingly, liver gene expression of
269 monoglyceride lipase (MGL), the rate-limiting enzyme in lipolysis, was only upregulated after
270 VFR in symptomatic male $APP^{NL-F}$ mice (Fig. 2B). This is one explanation for the decreased BW
271 and vWAT observed in this group. These data indicated that VFR in pre-symptomatic male
272 $APP^{NL-F}$ mice cause more ectopic liver lipids likely due to higher *de novo* lipogenesis, while the
273 contrary was observed in males at the symptomatic disease stage due to higher lipolysis.

274 <u>VFR in female $APP^{NL-F}$ mice led to increased gene expression of de novo lipogenesis and</u>
275 <u>decreased expression of lipolysis genes in reaccumulated vWAT.</u>

276 Nearly all the $APP^{NL-F}$ female mice reaccumulated vWAT after VFR, with similar morphology to
277 levels observed in sham surgery controls matched for age and sex (Fig. 1D, G). To understand
278 the reason for this reaccumulation, we examined gene expression of lipogenesis and lipolysis in
279 vWAT (Fig 2C). Expression levels of two key *de novo* lipogenesis genes, ACC and FAS, were
280 increased in $APP^{NL-F}$ female mice at either disease stage after VFR. The expression of ACC and
281 FAS were decreased following VFR in male $APP^{NL-F}$ mice at the symptomatic, but not at the pre-
282 symptomatic time point. Lipolysis gene expression, including protein kinase A (PKA), adipose
283 triglyceride lipase (ATGL), and hormone sensitive lipase (HSL), were decreased at both disease
284 stages after VFR in $APP^{NL-F}$ female mice compared with sham controls. In male mice, VFR
285 increased the expression of PKA, ATGL, and HSL at the pre-symptomatic, but unchanged, at
286 the symptomatic time point. The data suggests that the accumulation of vWAT after VFR in
287 female $APP^{NL-F}$ mice at either stage of disease progression is a result of increased lipogenesis
288 and decreased lipolysis gene expression. In male $APP^{NL-F}$ mice, the reduced accumulation of
289 vWAT after VFR was disease stage specific with pre-symptomatic time points increasing

290 expression of lipolysis genes, while surgery at the symptomatic time point decreased
291 lipogenesis gene expression. Interestingly, SREBP1 vWAT expression was upregulated after
292 VFR only in pre-symptomatic $APP^{NL-F}$ male mice. SREBP1 is a transcription factor activated by
293 high blood glucose (Bertolio et al., 2019, Zhao et al., 2024), suggesting altered glucose
294 metabolism in this cohort.

295 VFR surgery impacted either glucose tolerance or insulin sensitivity in male $APP^{NL-F}$ mice.

296 Lipid metabolism plays an important role in regulating glucose utilization, and the two processes
297 are tightly interconnected (Parhofer, 2015). Accordingly, the observed changes in lipid
298 metabolizing gene expression could affect glucose metabolism. To test the effects of VFR on
299 blood glucose metabolism, we monitored fasting and fed glucose levels as well as glucose
300 tolerance with a GTT, and insulin sensitivity with an ITT, at 18 months of age. VFR during the
301 pre-symptomatic disease stage in $APP^{NL-F}$ male mice reduced their glucose tolerance, but had
302 no effects in symptomatic males (Fig 3A). VFR improved insulin sensitivity in symptomatic
303 $APP^{NL-F}$ male mice, but effects were not observed during the pre-symptomatic stage in males
304 (Fig 3B). Consistent with the GTT, VFR increased fasting glucose in pre-symptomatic $APP^{NL-F}$
305 male mice compared with sham controls (Fig. 3C). VFR did not affect fasting blood glucose in
306 symptomatic $APP^{NL-F}$ male mice, nor were differences in fed glucose observed in either disease
307 stage of the male cohorts (Fig. 3D). Blood glucose levels were unchanged after VFR in either
308 disease stage of $APP^{NL-F}$ female mice.

309 The liver plays a major role in the control of whole body glucose homeostasis (Han et al., 2016,
310 Guerra and Gastaldelli, 2020, Scoditti et al., 2024). To understand the observed blood glucose
311 differences, we examined liver gene expression (Fig 4A) associated with gluconeogenesis
312 (synthesis of glucose from non-carbohydrate sources), glycolysis (breakdown of glucose for
313 energy), and glycogenesis (conversion of glucose to glycogen). VFR increased expression of
314 gluconeogenesis genes, glucose-6-phosphatase (G6PC) and phosphoenolpyruvate

315 carboxykinase (PEPCK), in pre-symptomatic male mice, consistent with their increased fasting
316 blood glucose levels (Fig 3C). In contrast, glucose transporter 2 (Glut2) was increased in
317 symptomatic males, while GCK (Glucokinase) and glycogen synthase 2 (GYS2) key genes in
318 glycolysis and glycogenesis, respectively, were decreased in female $APP^{NL-F}$ mice after VFR.

319 Taken together, the blood glucose and liver gene expression measures indicate VFR affected
320 glucose metabolism in a sex- and disease stage-dependent manner. Pre-symptomatic $APP^{NL-F}$
321 male mice had increased fasting blood glucose and made them less glucose tolerant after VFR,
322 likely mediated via increasing gluconeogenesis. At symptomatic time points, VFR improved
323 glucose metabolism by increasing insulin sensitivity via enhancing glycolytic and glycogenesis
324 gene expression. Although this gene expression was reduced after VFR in symptomatic female
325 mice, no effects on insulin sensitivity or blood glucose levels were observed.

326 <u>VFR alters plasma visfatin, adiponectin, and leptin in pre-symptomatic male $APP^{NL-F}$ mice.</u>

327 Adipokines secreted from adipose tissue are important for whole body glucose metabolism and
328 insulin sensitivity (Rabe et al., 2008, Kojta et al., 2020). Given the altered lipid and glucose
329 metabolism after VFR in the $APP^{NL-F}$ mice, we examined plasma adipokines. Visfatin is
330 primarily produced in vWAT, with plasma levels increasing in response to high-fat diet feeding
331 and obesity (Adeghate, 2008, Sethi and Vidal-Puig, 2005), and is associated with glucose
332 intolerance (Abdalla, 2022). VFR increased plasma visfatin in pre-symptomatic male $APP^{NL-F}$
333 mice compared with age-matched sham controls (Fig 4B), consistent with their higher ectopic
334 liver accumulation, fasting blood glucose, and glucose intolerance. No plasma visfatin
335 differences were observed in the other mouse cohorts.

336 Adiponectin enhances glucose and lipid metabolism (Yanai and Yoshida, 2019), decreases
337 lipogenesis (Richard et al., 2000), and has neuroprotective effects (Khoramipour et al., 2021).
338 VFR reduced plasma adiponectin in pre-symptomatic VFR $APP^{NL-F}$ male mice (Fig 4C). This

339 would also contribute to the reduced glucose metabolism and increased liver lipids observed in
340 this cohort. Plasma adiponectin changes were not observed after VFR in the other cohorts.

341 Leptin regulates appetite and energy expenditure, and its deficiency can disrupt glucose and
342 lipid metabolism, leading to neuronal damage that impairs neuroplasticity and memory
343 consolidation (Fernandes et al., 2024). Higher leptin levels are also associated with a lower
344 dementia risk (Lieb et al., 2009). Plasma leptin was decreased in pre-symptomatic $APP^{NL-F}$
345 male mice after VFR compared with age-matched sham controls (Fig. 4D). This likely
346 contributed to the imbalance of glucose and lipid metabolism in this male cohort. Differences in
347 plasma leptin levels were not observed in the other cohorts of mice.

348 <u>VFR increases WAT senescent cell and SASP markers in pre-symptomatic male and</u>
349 <u>symptomatic female $APP^{NL-F}$ mice.</u>

350 Adipose tissue, particularly vWAT, has the highest burden of senescent cells (Palmer et al.,
351 2021) and we previously showed senescent cell markers in vWAT were increased in male and
352 female $APP^{NL-F}$ mice (Fang et al., 2025). VFR can decrease systemic and neuroinflammation in
353 aged mice (Shin et al., 2015). We examined gene expression of senescent cell and SASP
354 markers in vWAT (Fig 5A). Gene expression of $p16^{Ink4\alpha}$, $p21^{Cip1}$, and IL-10 were increased in
355 vWAT after VFR in pre-symptomatic $APP^{NL-F}$ male mice. Expression of vWAT $p16^{Ink4\alpha}$ and
356 TNFα were also increased in symptomatic $APP^{NL-F}$ female mice (Fig 5A) while no differences in
357 IL-6 and MCP1 were observed in any cohort (data not shown) after VFR. SASP markers were
358 also examined in SubQ WAT where VFR increased TNFα, IL-10, IL-6, and MCP1 in pre-
359 symptomatic $APP^{NL-F}$ male mice (Fig 5B). SubQ IL-6 was also increased in symptomatic
360 $APP^{NL-F}$ female mice after VFR. Overall, VFR increased gene expression of senescent cell and
361 SASP markers in WAT of pre-symptomatic $APP^{NL-F}$ male mice, with a modest increase
362 observed in symptomatic females.

363 VFR modulates gene expression of hippocampal senescence, SASP, and cognitive markers.

364 Excess vWAT accumulation is linked to accelerated brain aging, neuroinflammation, and
365 dementia risk (Moser and Pike, 2016, Oh et al., 2023, Budamagunta et al., 2023). To
366 understand how VFR affected hippocampal function, the brain region strongly associated with
367 learning and memory, we examined gene expression of cell senescence and cytokines (Fig 6A).
368 VFR had no effect on $p16^{Ink4\alpha}$, $p21^{Cip1}$, or TNFα expression in $APP^{NL\text{-}F}$ male mice at either stage
369 of disease progression. Alternatively, $p16^{Ink4\alpha}$ gene expression was increased after VFR in pre-
370 symptomatic $APP^{NL\text{-}F}$ female mice. VFR caused a corresponding TNFα gene expression
371 increase in this cohort as well as the symptomatic females. VFR had deleterious effects on
372 hippocampal senescence and inflammation in female, but not male $APP^{NL\text{-}F}$ mice.

373 Since we observed improvements in object recognition memory after VFR in symptomatic male
374 $APP^{NL\text{-}F}$ mice, we examined markers associated with learning and memory in the hippocampus
375 (Fig 6A). Both adiponectin and leptin receptors (AdipoR, LepR) are found in the hippocampus
376 and play a role in synaptic plasticity and cognition. Gene expression of both receptors were
377 upregulated after VFR in symptomatic $APP^{NL\text{-}F}$ male mice (Fig 6A). In females, VFR increased
378 LepR in the pre-symptomatic disease stage. Cyclic AMP response element-binding protein 1
379 (Creb1), plays a role in long-term memory formation. VFR decreased Creb1 gene expression in
380 pre-symptomatic $APP^{NL\text{-}F}$ male mice, but elevated expression in the symptomatic male cohort.
381 Progranulin (PRGN) is important for neuronal survival and growth in the hippocampus. PRGN
382 gene expression was decreased after VFR in pre-symptomatic $APP^{NL\text{-}F}$ female mice, but elicited
383 an increase in symptomatic males. Overall, VFR altered the hippocampal gene expression
384 profile of symptomatic $APP^{NL\text{-}F}$ male mice in a manner that would improve their object
385 recognition memory.

386 VFR increases soluble $A\beta_{42}$ in pre-symptomatic male and female mice.

387 Soluble $A\beta_{42}$ is the neurotoxic species associated with synaptic dysfunction and cognitive
388 decline in AD (Findley et al., 2019). An ELISA indicated hippocampal soluble $A\beta_{42}$ (Fig 6B)
389 production was only increased in pre-symptomatic stage of $APP^{NL\text{-}F}$ male and female mice after
390 VFR. VFR did not affect soluble $A\beta_{42}$ during the symptomatic stage in either sex.

391 **Discussion**

392 Adipose tissue accumulation and distribution exhibit sex-specific differences, yet these patterns
393 are evolutionarily conserved across humans and mice (Chusyd et al., 2016). Females typically
394 have a higher overall fat percentage with a large proportion stored subcutaneously for energy
395 supply during pregnancy and lactation during food scarcity, while males accumulate fat in
396 visceral regions. Numerous variables influence adipose development including sex
397 chromosomes, gonadal hormone levels, and hormone receptors. Sex chromosome complement
398 impacts adipose accumulation whereby the presence of two "X" chromosomes leads to higher
399 accumulation while the presence of the "Y" chromosome has no influence. The gonadal
400 hormones, testosterone and estrogen, drive vWAT and SubQ accumulation in males and
401 females, respectively. Age-related hormonal changes increase vWAT accumulation regardless
402 of sex and is a key factor in the development of metabolic syndrome that increases dementia
403 risk.

404 Besides its role as an energy reservoir, adipose tissue is an endocrine organ that secretes
405 peptides such as TNFα, IL-6, and adiponectin, which can influence either tissue-specific or
406 whole body metabolism. Prior studies examining VFR effects in rodents were conducted to
407 elucidate mechanisms contributing to metabolic improvements. VFR improves insulin sensitivity
408 and glucose tolerance in young, aged, and obese rodents with some of the metabolic changes
409 occurring through decreased free fatty acids, leptin, and TNFα expression (Kim et al., 1999,
410 Gabriely et al., 2002, Shi et al., 2007a). VFR in aged C57BL/6 mice led to reduced expression
411 of pro-inflammatory cytokines in the plasma, WAT, and cortex (Shin et al., 2015). Although
412 adiponectin plays a key role in glucose and lipid metabolism and suppresses inflammatory
413 cytokines, serum levels are found to decrease following VFR in male and female Sprague
414 Dawley rats (Borst et al., 2005, Ling et al., 2014), which may be due to the absence of these

415 WAT depots. Considering the metabolic benefits of VFR and the known link between metabolic
416 dysfunction and AD risk, we aimed to investigate the impact of VFR in an AD model.

417 Surprisingly, the VFR response was disease stage- and sex-dependent. The removal of vWAT
418 in symptomatic $APP^{NL-F}$ male mice improved object recognition memory potentially due to
419 increased hippocampal AdipoR, LepR, Creb1, and PRGN expression. Lipogenesis vWAT gene
420 expression was down-regulated, while hepatic genes associated with lipolysis and glucose
421 transport were up-regulated. These effects were associated with a decreased percentage of
422 total liver lipids. All of these alterations were reflected by a reduced percentage of total fat,
423 specifically reaccumulated vWAT, BW, and improved blood glucose maintenance. The opposite
424 was true for VFR during the pre-symptomatic stage in males. After VFR, an imbalance of lipid
425 metabolism was prevalent, reflected by an elevated expression of vWAT lipolysis and hepatic
426 lipogenesis genes. This tissue metabolic imbalance may be a result of adipocyte hyperplasia
427 with reduced cell size as well as the redistribution of lipids into other organs, such as the liver,
428 where higher ectopic fat accumulation was observed. Plasma adiponectin and leptin were
429 decreased along with increased visfatin resulting in impaired glucose metabolism and peripheral
430 inflammation. Typically, adiponectin and leptin are inversely related, but plasma levels of both
431 were decreased in pre-symptomatic male $APP^{NL-F}$ mice. The decrease in leptin might be due to
432 the loss of the adipose depot while the anticipated compensatory increase in adiponectin may
433 not have been observed because the adiponectin source was also depleted. Further studies are
434 needed to determine why this effect was not observed in the other cohorts after VFR. In the
435 brain, reduced hippocampal Creb1 expression and increased soluble $A\beta_{42}$, combined with the
436 aforementioned adverse physiological changes, failed to improve object recognition memory.

437 In contrast to males, vWAT reaccumulated in nearly all female mice and was similar in number
438 and size to sham littermates regardless of when VFR occurred. This could be attributed to
439 higher lipogenesis and lower lipolysis gene expression. Although ectopic lipid deposition did not

440 accumulate in the liver, VFR in pre-symptomatic female $APP^{NL-F}$ mice led to decreased hepatic
441 lipogenesis gene expression, while expression of genes involved in glycolysis and glycogenesis
442 were decreased in symptomatic females. These results were in opposition to age-matched
443 males. Hippocampal soluble $A\beta_{42}$, senescent cell, and inflammatory markers were elevated in
444 pre-symptomatic $APP^{NL-F}$ female mice while the later was only observed at the symptomatic
445 time point. No changes to blood glucose levels or object recognition memory were observed in
446 females after VFR.

447 Lipectomy in mice, rats, and other small mammals does not result in long-term BW loss with
448 regain occurring 12-14 weeks post-surgery (Murillo et al., 2019). In the majority of the studies
449 this was attributed to regeneration of the lipectomized depot, redistribution of fat to other
450 adipose depots, or ectopic fat accumulation in other organs. In our present study, female
451 $APP^{NL-F}$ mice regained BW due to reaccumulating vWAT. Although vWAT accumulation was
452 lower in pre-symptomatic males, they regained BW due to ectopic fat distribution in the liver and
453 possibly other organs. Only symptomatic $APP^{NL-F}$ male mice had lower BW attributed to less
454 visceral adiposity. Redistribution of fat to other adipose depots was not observed in any cohort.
455 Our present study was designed to examine disease stage-specific interventional or therapeutic
456 AD strategies rather than examining the contribution of aging on adiposity and AD progression.
457 Regardless, effects of aging on adipose accumulation likely contributed to the observed
458 differences in lipid distribution and the comparable end-of-study BW between sham and VFR
459 cohorts matched for age and sex. The gradual decline in estrous cycling and the associated
460 drop in estrogen levels, which promotes visceral rather than SubQ accumulation, may partially
461 explain post-resection visceral accumulation in female mice, whereas aging males exhibit
462 ectopic liver lipid deposition (Donato et al., 2014).

463 The exact mechanisms behind this adipose rebound are not well known, but suggest biological
464 feedback systems that act to preserve energy balance. For example, the adipostat hypothesis

465 postulates that alterations to energy reserves triggers compensatory mechanisms in metabolism
466 and/or thermogenesis to restore the reservoir. Since gonadal hormones and sex chromosome
467 complement mediate adipose storage, distribution, and utilization, male and female mice use
468 different behavioral strategies to restore fat after lipectomy. Males increase caloric consumption
469 while females reduce heat production and energy expenditure (Shi et al., 2007b). Our findings
470 are in support of this whereby pre-symptomatic $APP^{NL-F}$ male mice had increased
471 gluconeogenesis gene expression and fasting blood glucose, and worse glucose tolerance after
472 VFR. While VFR in Female $APP^{NL-F}$ mice reduced glycolysis and lipolysis, but increased
473 lipogenesis gene expression. It is important to note, however, that our study was not intended
474 to serve as a preclinical model for liposuction, as that procedure primarily targets SubQ rather
475 than vWAT depots. However, lipectomy in humans causes a transient decrease in BW and
476 adipose depots that gradually return to preoperative levels within months (Hernandez et al.,
477 2011, Seretis et al., 2015), suggesting the preservation of this energy balance is conserved
478 across species.

479 The accumulation of WAT and subsequent increases in BW begins in midlife and continues into
480 early aging in both humans (40-65 years) and mice (12-18 months). The reason for this
481 increase is attributed to adipogenesis and adipocyte hypertrophy that are prominent during
482 midlife (Wang et al., 2025). Remodeling of vWAT, like its distribution, varies between sexes,
483 with estrogen levels playing a key role in regulating these processes and shifting notably with
484 age. Female mice have increased adipose progenitor cells leading to hyperplasia while males
485 experience hypertrophy (Wu et al., 2017). Both increase adipose accumulation, but hyperplasia
486 is associated with better metabolic health (Steiner and Berry, 2022), which may explain why
487 blood glucose levels were unaffected in female mice after VFR. Hypertrophic adipocytes
488 secrete reduced adiponectin and increased pro-inflammatory cytokines, the latter promoting
489 ectopic lipid distribution into peripheral organs. These pathological features were evident

following VFR in pre-symptomatic $APP^{NL-F}$ male mice, despite the reaccumulated vWAT exhibiting a less hypertrophic phenotype. Accordingly, adipose cell size rather than number correlates with increased risk for metabolic syndrome (Vishvanath and Gupta, 2019).

Senescent cell accumulation in both the periphery and brain contribute to aging and age-related neurodegenerative disorders such as AD. The mechanisms behind this are multifaceted and dependent upon the type of senescent cell (Zhu et al., 2024). Senescent brain cells alter amyloid precursor protein processing by shifting it from the non-amyloidogenic to the amyloidogenic pathway, promoting the formation of Aβ (Sun et al., 2018). The pro-inflammatory SASP response coupled with decreased microglial phagocytosis of misfolded proteins can lead to the subsequent Aβ accumulation and deposition in the brain. We observed elevated hippocampal soluble $A\beta_{42}$ after VFR in pre-symptomatic $APP^{NL-F}$ mice compared with sex-matched sham controls, which was contradictory to our hypothesis. VFR increased WAT senescent cell burden and SASP in pre-symptomatic males, while these were increased in the hippocampus of pre-symptomatic females. Considering senescent cell and SASP increases were predominantly observed in the pre-symptomatic groups, this may indicate a long-term effect of VFR. In AD mouse models, reducing peripheral and hippocampal senescent cell burden with senolytics has been shown to reduce amyloid pathology and improve cognitive performance - albeit with benefits favoring female mice (Currais et al., 2014, Zhang et al., 2019, Fang et al., 2025, Ng et al., 2024).

Given that AD pathology is thought to initiate in midlife prior to cognitive decline, the concurrent increase in adipose tissue accumulation during this period may play a causal role in disease progression. Our present study indicates accumulation or redistribution of adipose tissue during the pre-symptomatic AD stage can cause metabolic disturbances resulting in sex-specific peripheral and cerebral senescent cell accumulation that exacerbates pathological AD progression. However, during symptomatic AD stages, elimination of vWAT has beneficial

515 metabolic and cognitive effects in male, but not female $APP^{NL-F}$ mice. These sex-specific
516 differences are attributed to increasing energy storage in female symptomatic mice.

517 Several study limitations should be noted when interpreting the results of the present study.
518 Although the study design was focused on identifying within-model sex-specific and disease-
519 stage dependent alterations relevant for ameliorating AD progression; inclusion of age-matched
520 genetic background control C57BL/6 mice could enhance the interpretability and translational
521 relevance of the findings. Second, we did not measure circulating gonadal hormones since our
522 study design did not include repeated sampling or estrous cycle staging. A single-point
523 hormone measurement would not have yielded biologically meaningful data due to the large
524 physiological variability inherent in their sampling. Third, we only measured ectopic lipid
525 deposition in the liver, so therefore it is possible for lipids to accumulate in other organs such as
526 muscle. Finally, we focused on specific comparisons of sham and VFR surgery animals to their
527 age- and sex-matched controls, consistent with the hypothesis, by means of a t-test. This was
528 done to avoid exploratory-type findings for possible age and sex effects since our primary goal
529 was to assess whether VFR improved cognitive performance at distinct disease stages within
530 each sex.
531

532 **Disclosures**

533 The authors state that they have no financial or non-financial competing interests to disclose.
534 SAM, YF, MRP, KQ, TH, and JEC conducted the experiments and analyzed the data. YF, AB,
535 KNH, and ERH conceived the study, designed the experiments, interpreted the data, and wrote
536 the manuscript. All authors approved the final version of the manuscript.
537

538 **Funding Sources**

This work was supported by the National Institutes of Health NIA R01-AG057767 and NIA R01-AG061937, Kenneth Stark Endowment, and Dale and Deborah Smith Center for Alzheimer's Research and Treatment (YF, MRP, KQ, JEC, SM, TH, KNH, ERH). Geriatrics Initiative (AB).

543 **References**


544 ABDALLA, M. M. I. 2022. Role of visfatin in obesity-induced insulin resistance. *World J Clin Cases,* 10**,**
545 10840-10851.
546 ABI-GHANEM, C., KELLY, R. D., GROOM, E. A., VALERIAN, C. G., PAUL, A. S., THRASHER, C. A., SALINERO,
547 A. E., BATCHELDER, M. R., LAFRICAN, J. J., WANG, M., SMITH, R. M., TEMPLE, S., ZULOAGA, D. G.
548 & ZULOAGA, K. L. 2025. Interactions between menopause and high-fat diet on cognition and
549 pathology in a mouse model of Alzheimer's disease. *Alzheimers Dement,* 21**,** e70026.
550 ADEGHATE, E. 2008. Visfatin: structure, function and relation to diabetes mellitus and other
551 dysfunctions. *Curr Med Chem,* 15**,** 1851-62.
552 BAGLIETTO-VARGAS, D., SHI, J., YAEGER, D. M., AGER, R. & LAFERLA, F. M. 2016. Diabetes and
553 Alzheimer's disease crosstalk. *Neurosci Biobehav Rev,* 64**,** 272-87.
554 BARZILAI, N., SHE, L., LIU, L., WANG, J., HU, M., VUGUIN, P. & ROSSETTI, L. 1999. Decreased visceral
555 adiposity accounts for leptin effect on hepatic but not peripheral insulin action. *Am J Physiol,*
556 277**,** E291-8.
557 BENITEZ, D. P., JIANG, S., WOOD, J., WANG, R., HALL, C. M., PEERBOOM, C., WONG, N., STRINGER, K. M.,
558 VITANOVA, K. S., SMITH, V. C., JOSHI, D., SAITO, T., SAIDO, T. C., HARDY, J., HANRIEDER, J., DE
559 STROOPER, B., SALIH, D. A., TRIPATHI, T., EDWARDS, F. A. & CUMMINGS, D. M. 2021. Knock-in
560 models related to Alzheimer's disease: synaptic transmission, plaques and the role of microglia.
561 *Mol Neurodegener,* 16**,** 47.
562 BERTOLIO, R., NAPOLETANO, F., MANO, M., MAURER-STROH, S., FANTUZ, M., ZANNINI, A., BICCIATO, S.,
563 SORRENTINO, G. & DEL SAL, G. 2019. Sterol regulatory element binding protein 1 couples
564 mechanical cues and lipid metabolism. *Nat Commun,* 10**,** 1326.
565 BIESSELS, G. J. & DESPA, F. 2018. Cognitive decline and dementia in diabetes mellitus: mechanisms and
566 clinical implications. *Nat Rev Endocrinol,* 14**,** 591-604.
567 BORST, S. E., CONOVER, C. F. & BAGBY, G. J. 2005. Association of resistin with visceral fat and muscle
568 insulin resistance. *Cytokine,* 32**,** 39-44.
569 BREIJYEH, Z. & KARAMAN, R. 2020. Comprehensive Review on Alzheimer's Disease: Causes and
570 Treatment. *Molecules,* 25.
571 BUDAMAGUNTA, V., KUMAR, A., RANI, A., BEAN, L., MANOHAR-SINDHU, S., YANG, Y., ZHOU, D. &
572 FOSTER, T. C. 2023. Effect of peripheral cellular senescence on brain aging and cognitive decline.
573 *Aging Cell,* 22**,** e13817.
574 CHUSYD, D. E., WANG, D., HUFFMAN, D. M. & NAGY, T. R. 2016. Relationships between Rodent White
575 Adipose Fat Pads and Human White Adipose Fat Depots. *Front Nutr,* 3**,** 10.
576 CURRAIS, A., PRIOR, M., DARGUSCH, R., ARMANDO, A., EHREN, J., SCHUBERT, D., QUEHENBERGER, O. &
577 MAHER, P. 2014. Modulation of p25 and inflammatory pathways by fisetin maintains cognitive
578 function in Alzheimer's disease transgenic mice. *Aging Cell,* 13**,** 379-90.
579 DONATO, A. J., HENSON, G. D., HART, C. R., LAYEC, G., TRINITY, J. D., BRAMWELL, R. C., ENZ, R. A.,
580 MORGAN, R. G., REIHL, K. D., HAZRA, S., WALKER, A. E., RICHARDSON, R. S. & LESNIEWSKI, L. A.
581 2014. The impact of ageing on adipose structure, function and vasculature in the B6D2F1
582 mouse: evidence of significant multisystem dysfunction. *J Physiol,* 592**,** 4083-96.
583 DOVE, A., SHANG, Y., XU, W., GRANDE, G., LAUKKA, E. J., FRATIGLIONI, L. & MARSEGLIA, A. 2021. The
584 impact of diabetes on cognitive impairment and its progression to dementia. *Alzheimers*
585 *Dement,* 17**,** 1769-1778.
586 ELIAS, M. F., ELIAS, P. K., SULLIVAN, L. M., WOLF, P. A. & D'AGOSTINO, R. B. 2005. Obesity, diabetes and
587 cognitive deficit: The Framingham Heart Study. *Neurobiol Aging,* 26 Suppl 1**,** 11-6.

588 FANG, Y., MCFADDEN, S., DARCY, J., HASCUP, E. R., HASCUP, K. N. & BARTKE, A. 2020. Lifespan of long-
589 lived growth hormone receptor knockout mice was not normalized by housing at 30 degrees C
590 since weaning. *Aging Cell,* 19**,** e13123.
591 FANG, Y., MEDINA, D., STOCKWELL, R., MCFADDEN, S., QUINN, K., PECK, M. R., BARTKE, A., HASCUP, K.
592 N. & HASCUP, E. R. 2023. Sexual dimorphic metabolic and cognitive responses of C57BL/6 mice
593 to Fisetin or Dasatinib and quercetin cocktail oral treatment. *Geroscience,* 45**,** 2835-2850.
594 FANG, Y., PECK, M. R., QUINN, K., CHAPMAN, J. E., MEDINA, D., MCFADDEN, S. A., BARTKE, A., HASCUP,
595 E. R. & HASCUP, K. N. 2025. Senolytic intervention improves cognition, metabolism, and
596 adiposity in female APP(NL)(-F/NL-F) mice. *Geroscience,* 47**,** 1123-1138.
597 FERNANDES, C., FORNY-GERMANO, L., ANDRADE, M. M., LYRA, E. S. N. M., RAMOS-LOBO, A. M.,
598 MEIRELES, F., TOVAR-MOLL, F., HOUZEL, J. C., DONATO, J., JR. & DE FELICE, F. G. 2024. Leptin
599 receptor reactivation restores brain function in early-life Lepr-deficient mice. *Brain,* 147**,** 2706-
600 2717.
601 FINDLEY, C. A., BARTKE, A., HASCUP, K. N. & HASCUP, E. R. 2019. Amyloid Beta-Related Alterations to
602 Glutamate Signaling Dynamics During Alzheimer's Disease Progression. *ASN Neuro,* 11**,**
603 1759091419855541.
604 FOSTER, M. T., SHI, H., SEELEY, R. J. & WOODS, S. C. 2011. Removal of intra-abdominal visceral adipose
605 tissue improves glucose tolerance in rats: role of hepatic triglyceride storage. *Physiol Behav,*
606 104**,** 845-54.
607 FRANCZYK, M. P., HE, M. & YOSHINO, J. 2021. Removal of Epididymal Visceral Adipose Tissue Prevents
608 Obesity-Induced Multi-organ Insulin Resistance in Male Mice. *J Endocr Soc,* 5**,** bvab024.
609 GABRIELY, I., MA, X. H., YANG, X. M., ATZMON, G., RAJALA, M. W., BERG, A. H., SCHERER, P., ROSSETTI, L.
610 & BARZILAI, N. 2002. Removal of visceral fat prevents insulin resistance and glucose intolerance
611 of aging: an adipokine-mediated process? *Diabetes,* 51**,** 2951-8.
612 GUERRA, S. & GASTALDELLI, A. 2020. The role of the liver in the modulation of glucose and insulin in non
613 alcoholic fatty liver disease and type 2 diabetes. *Curr Opin Pharmacol,* 55**,** 165-174.
614 GUO, D. H., YAMAMOTO, M., HERNANDEZ, C. M., KHODADADI, H., BABAN, B. & STRANAHAN, A. M.
615 2020. Visceral adipose NLRP3 impairs cognition in obesity via IL-1R1 on CX3CR1+ cells. *J Clin*
616 *Invest,* 130**,** 1961-1976.
617 GUSTAFSON, D. R. 2012. Adiposity and cognitive decline: underlying mechanisms. *J Alzheimers Dis,* 30
618 Suppl 2**,** S97-112.
619 HAN, H. S., KANG, G., KIM, J. S., CHOI, B. H. & KOO, S. H. 2016. Regulation of glucose metabolism from a
620 liver-centric perspective. *Exp Mol Med,* 48**,** e218.
621 HERNANDEZ, T. L., KITTELSON, J. M., LAW, C. K., KETCH, L. L., STOB, N. R., LINDSTROM, R. C.,
622 SCHERZINGER, A., STAMM, E. R. & ECKEL, R. H. 2011. Fat redistribution following suction
623 lipectomy: defense of body fat and patterns of restoration. *Obesity (Silver Spring),* 19**,** 1388-95.
624 HUANG, X., WANG, Y. J. & XIANG, Y. 2022. Bidirectional communication between brain and visceral
625 white adipose tissue: Its potential impact on Alzheimer's disease. *EBioMedicine,* 84**,** 104263.
626 KAMOGAWA, K., KOHARA, K., TABARA, Y., UETANI, E., NAGAI, T., YAMAMOTO, M., IGASE, M. & MIKI, T.
627 2010. Abdominal fat, adipose-derived hormones and mild cognitive impairment: the J-SHIPP
628 study. *Dement Geriatr Cogn Disord,* 30**,** 432-9.
629 KHORAMIPOUR, K., CHAMARI, K., HEKMATIKAR, A. A., ZIYAIYAN, A., TAHERKHANI, S., ELGUINDY, N. M. &
630 BRAGAZZI, N. L. 2021. Adiponectin: Structure, Physiological Functions, Role in Diseases, and
631 Effects of Nutrition. *Nutrients,* 13.
632 KIM, S., YI, H. A., WON, K. S., LEE, J. S. & KIM, H. W. 2022. Association between Visceral Adipose Tissue
633 Metabolism and Alzheimer's Disease Pathology. *Metabolites,* 12.

634 KIM, Y. W., KIM, J. Y. & LEE, S. K. 1999. Surgical removal of visceral fat decreases plasma free fatty acid
635 and increases insulin sensitivity on liver and peripheral tissue in monosodium glutamate (MSG)-
636 obese rats. *J Korean Med Sci,* 14**,** 539-45.
637 KOJTA, I., CHACINSKA, M. & BLACHNIO-ZABIELSKA, A. 2020. Obesity, Bioactive Lipids, and Adipose Tissue
638 Inflammation in Insulin Resistance. *Nutrients,* 12.
639 LIEB, W., BEISER, A. S., VASAN, R. S., TAN, Z. S., AU, R., HARRIS, T. B., ROUBENOFF, R., AUERBACH, S.,
640 DECARLI, C., WOLF, P. A. & SESHADRI, S. 2009. Association of plasma leptin levels with incident
641 Alzheimer disease and MRI measures of brain aging. *JAMA,* 302**,** 2565-72.
642 LING, B. L., CHIU, C. T., LU, H. C., LIN, J. J., KUO, C. Y. & CHOU, F. P. 2014. Short and long-term impact of
643 lipectomy on expression profile of hepatic anabolic genes in rats: a high fat and high cholesterol
644 diet-induced obese model. *PLoS One,* 9**,** e108717.
645 MASTERNAK, M. M., BARTKE, A., WANG, F., SPONG, A., GESING, A., FANG, Y., SALMON, A. B., HUGHES, L.
646 F., LIBERATI, T., BOPARAI, R., KOPCHICK, J. J. & WESTBROOK, R. 2012. Metabolic effects of intra-
647 abdominal fat in GHRKO mice. *Aging Cell,* 11**,** 73-81.
648 MOSER, V. A. & PIKE, C. J. 2016. Obesity and sex interact in the regulation of Alzheimer's disease.
649 *Neurosci Biobehav Rev,* 67**,** 102-18.
650 MURILLO, A. L., KAISER, K. A., SMITH, D. L., JR., PETERSON, C. M., AFFUSO, O., TIWARI, H. K. & ALLISON,
651 D. B. 2019. A Systematic Scoping Review of Surgically Manipulated Adipose Tissue and the
652 Regulation of Energetics and Body Fat in Animals. *Obesity (Silver Spring),* 27**,** 1404-1417.
653 NG, P. Y., ZHANG, C., LI, H. & BAKER, D. J. 2024. Senescence Targeting Methods Impact Alzheimer's
654 Disease Features in 3xTg Mice. *J Alzheimers Dis,* 97**,** 1751-1763.
655 NGUYEN, J. C., KILLCROSS, A. S. & JENKINS, T. A. 2014. Obesity and cognitive decline: role of
656 inflammation and vascular changes. *Front Neurosci,* 8**,** 375.
657 OH, H. S., RUTLEDGE, J., NACHUN, D., PALOVICS, R., ABIOSE, O., MORAN-LOSADA, P., CHANNAPPA, D.,
658 UREY, D. Y., KIM, K., SUNG, Y. J., WANG, L., TIMSINA, J., WESTERN, D., LIU, M., KOHLFELD, P.,
659 BUDDE, J., WILSON, E. N., GUEN, Y., MAURER, T. M., HANEY, M., YANG, A. C., HE, Z., GREICIUS,
660 M. D., ANDREASSON, K. I., SATHYAN, S., WEISS, E. F., MILMAN, S., BARZILAI, N., CRUCHAGA, C.,
661 WAGNER, A. D., MORMINO, E., LEHALLIER, B., HENDERSON, V. W., LONGO, F. M.,
662 MONTGOMERY, S. B. & WYSS-CORAY, T. 2023. Organ aging signatures in the plasma proteome
663 track health and disease. *Nature,* 624**,** 164-172.
664 PALMER, A. K., TCHKONIA, T. & KIRKLAND, J. L. 2021. Senolytics: Potential for Alleviating Diabetes and Its
665 Complications. *Endocrinology,* 162.
666 PARHOFER, K. G. 2015. Interaction between Glucose and Lipid Metabolism: More than Diabetic
667 Dyslipidemia. *Diabetes Metab J,* 39**,** 353-62.
668 PETERSEN, M. C. & SHULMAN, G. I. 2018. Mechanisms of Insulin Action and Insulin Resistance. *Physiol*
669 *Rev,* 98**,** 2133-2223.
670 PITOMBO, C., ARAUJO, E. P., DE SOUZA, C. T., PAREJA, J. C., GELONEZE, B. & VELLOSO, L. A. 2006.
671 Amelioration of diet-induced diabetes mellitus by removal of visceral fat. *J Endocrinol,* 191**,** 699-
672 706.
673 RABE, K., LEHRKE, M., PARHOFER, K. G. & BROEDL, U. C. 2008. Adipokines and insulin resistance. *Mol*
674 *Med,* 14**,** 741-51.
675 RICHARD, A. J., WHITE, U., ELKS, C. M. & STEPHENS, J. M. 2000. Adipose Tissue: Physiology to Metabolic
676 Dysfunction. *In:* FEINGOLD, K. R., AHMED, S. F., ANAWALT, B., BLACKMAN, M. R., BOYCE, A.,
677 CHROUSOS, G., CORPAS, E., DE HERDER, W. W., DHATARIYA, K., DUNGAN, K., HOFLAND, J.,
678 KALRA, S., KALTSAS, G., KAPOOR, N., KOCH, C., KOPP, P., KORBONITS, M., KOVACS, C. S.,
679 KUOHUNG, W., LAFERRERE, B., LEVY, M., MCGEE, E. A., MCLACHLAN, R., MUZUMDAR, R.,
680 PURNELL, J., REY, R., SAHAY, R., SHAH, A. S., SINGER, F., SPERLING, M. A., STRATAKIS, C. A.,
681 TRENCE, D. L. & WILSON, D. P. (eds.) *Endotext.* South Dartmouth (MA).

682 SAITO, T., MATSUBA, Y., MIHIRA, N., TAKANO, J., NILSSON, P., ITOHARA, S., IWATA, N. & SAIDO, T. C.
683 2014. Single App knock-in mouse models of Alzheimer's disease. *Nat Neurosci,* 17**,** 661-3.
684 SAKERS, A., DE SIQUEIRA, M. K., SEALE, P. & VILLANUEVA, C. J. 2022. Adipose-tissue plasticity in health
685 and disease. *Cell,* 185**,** 419-446.
686 SCODITTI, E., SABATINI, S., CARLI, F. & GASTALDELLI, A. 2024. Hepatic glucose metabolism in the
687 steatotic liver. *Nat Rev Gastroenterol Hepatol,* 21**,** 319-334.
688 SERETIS, K., GOULIS, D. G., KOLIAKOS, G. & DEMIRI, E. 2015. Short- and Long-Term Effects of Abdominal
689 Lipectomy on Weight and Fat Mass in Females: a Systematic Review. *Obes Surg,* 25**,** 1950-8.
690 SETHI, J. K. & VIDAL-PUIG, A. 2005. Visfatin: the missing link between intra-abdominal obesity and
691 diabetes? *Trends Mol Med,* 11**,** 344-7.
692 SHI, H., STRADER, A. D., WOODS, S. C. & SEELEY, R. J. 2007a. The effect of fat removal on glucose
693 tolerance is depot specific in male and female mice. *Am J Physiol Endocrinol Metab,* 293**,** E1012-
694 20.
695 SHI, H., STRADER, A. D., WOODS, S. C. & SEELEY, R. J. 2007b. Sexually dimorphic responses to fat loss
696 after caloric restriction or surgical lipectomy. *Am J Physiol Endocrinol Metab,* 293**,** E316-26.
697 SHIN, J. A., JEONG, S. I., KIM, M., YOON, J. C., KIM, H. S. & PARK, E. M. 2015. Visceral adipose tissue
698 inflammation is associated with age-related brain changes and ischemic brain damage in aged
699 mice. *Brain Behav Immun,* 50**,** 221-231.
700 ST-ONGE, M. P. & GALLAGHER, D. 2010. Body composition changes with aging: the cause or the result of
701 alterations in metabolic rate and macronutrient oxidation? *Nutrition,* 26**,** 152-5.
702 STEINER, B. M. & BERRY, D. C. 2022. The Regulation of Adipose Tissue Health by Estrogens. *Front*
703 *Endocrinol (Lausanne),* 13**,** 889923.
704 SUN, R., HE, T., PAN, Y. & KATUSIC, Z. S. 2018. Effects of senescence and angiotensin II on expression and
705 processing of amyloid precursor protein in human cerebral microvascular endothelial cells.
706 *Aging (Albany NY),* 10**,** 100-114.
707 TCHKONIA, T., MORBECK, D. E., VON ZGLINICKI, T., VAN DEURSEN, J., LUSTGARTEN, J., SCRABLE, H.,
708 KHOSLA, S., JENSEN, M. D. & KIRKLAND, J. L. 2010. Fat tissue, aging, and cellular senescence.
709 *Aging Cell,* 9**,** 667-84.
710 TRAN, T. M., DAI, T. X. T., TRAN, D. B., NGUYEN, Q. C. T. & NGUYEN, D. H. Y. 2019. A simple
711 spectrophotometric method for quantifying total lipids in plants and animals. *CTU Journal of*
712 *Innovation and Sustainable Development,* 11**,** 106-110.
713 VISHVANATH, L. & GUPTA, R. K. 2019. Contribution of adipogenesis to healthy adipose tissue expansion
714 in obesity. *J Clin Invest,* 129**,** 4022-4031.
715 WANG, G., LI, G., SONG, A., ZHAO, Y., YU, J., WANG, Y., DAI, W., SALAS, M., QIN, H., MEDRANO, L., DOW,
716 J., LI, A., ARMSTRONG, B., FUEGER, P. T., YU, H., ZHU, Y., SHAO, M., WU, X., JIANG, L., CAMPISI,
717 J., YANG, X. & WANG, Q. A. 2025. Distinct adipose progenitor cells emerging with age drive
718 active adipogenesis. *Science,* 388**,** eadj0430.
719 WHITMER, R. A., GUSTAFSON, D. R., BARRETT-CONNOR, E., HAAN, M. N., GUNDERSON, E. P. & YAFFE, K.
720 2008. Central obesity and increased risk of dementia more than three decades later. *Neurology,*
721 71**,** 1057-64.
722 WONG ZHANG, D. E., TRAN, V., VINH, A., DINH, Q. N., DRUMMOND, G. R., SOBEY, C. G., JELINIC, M. & DE
723 SILVA, T. M. 2023. Pathophysiological Links Between Obesity and Dementia. *Neuromolecular*
724 *Med,* 25**,** 451-456.
725 WU, Y., LEE, M. J., IDO, Y. & FRIED, S. K. 2017. High-fat diet-induced obesity regulates MMP3 to
726 modulate depot- and sex-dependent adipose expansion in C57BL/6J mice. *Am J Physiol*
727 *Endocrinol Metab,* 312**,** E58-E71.
728 YANAI, H. & YOSHIDA, H. 2019. Beneficial Effects of Adiponectin on Glucose and Lipid Metabolism and
729 Atherosclerotic Progression: Mechanisms and Perspectives. *Int J Mol Sci,* 20.

730 ZHANG, P., KISHIMOTO, Y., GRAMMATIKAKIS, I., GOTTIMUKKALA, K., CUTLER, R. G., ZHANG, S.,
731 ABDELMOHSEN, K., BOHR, V. A., MISRA SEN, J., GOROSPE, M. & MATTSON, M. P. 2019. Senolytic
732 therapy alleviates Abeta-associated oligodendrocyte progenitor cell senescence and cognitive
733 deficits in an Alzheimer's disease model. *Nat Neurosci,* 22**,** 719-728.
734 ZHAO, Z., XIANG, X., CHEN, Q., DU, J., ZHU, S., XU, X., SHEN, Y., WEN, S., LI, Y., XU, W., MAI, K. & AI, Q.
735 2024. Sterol Regulatory Element Binding Protein 1: A Mediator for High-Fat Diet-Induced
736 Hepatic Gluconeogenesis and Glucose Intolerance in Fish. *J Nutr,* 154**,** 1505-1516.
737 ZHU, J., WU, C. & YANG, L. 2024. Cellular senescence in Alzheimer's disease: from physiology to
738 pathology. *Transl Neurodegener,* 13**,** 55.

739

740 **Figure Legends**

741 *Figure 1 - NOR and body composition analysis after VFR*. The retention index (A) and novelty
742 preference (B) for the NOR task were calculated at 18 months of age for all groups. BW (C) and
743 the percentage of vWAT (D) and total fat mass for BAT, SubQ, and vWAT (E) in relation to BW
744 were determined upon euthanization at 19 months of age. The percentage of VFR mice that
745 regenerated vWAT (reg. ratio) are shown in (D). Representative 40x images of H&E stained
746 vWAT in pre-symptomatic male sham (top) and VFR (bottom) cohorts (F). The average number
747 of vWAT adipocytes and their internal diameter were determined for all groups (G). Data are
748 represented as means ± SEM. *p<0.05, **p<0.01 based on a two-tailed Welch's *t* test (A-C, E),
749 a two-way ANOVA with Sidak's post hoc (D), and an unpaired two-tailed t test (G); n=4-20.

750 *Figure 2 – Lipid metabolism in hepatic and vWAT.* The sulfo-phospho-vanillin method was used
751 to measure the percentage of total liver lipids (A). qRT-PCR was used to determine relative
752 gene expression profile of lipolysis and lipogenesis genes in the liver (B) and vWAT (C). Data
753 are represented as means ± SEM. *p<0.05, **p<0.01, ***p<0.001, ****p<0.0001 based on a two-
754 tailed Welch's t test (n=8-15). Abbreviations: ACC – acetyl CoA-carboxylase, FAS – fatty acid
755 synthase, SCD1 - stearoyl-CoA Desaturase, Elovl6 – fatty acid elongase enzyme 6, SREBP1 –
756 sterol regulatory element-binding protein 1, MGL – monoglyceride lipase, PKA – protein kinase
757 A, ATGL – adipose triglyceride lipase, HSL – hormone sensitive lipase

758 *Figure 3 – Blood glucose levels in pre-symptomatic and symptomatic $APP^{NL-F}$ mice.* Mice were
759 fasted for 15 hours before they received an ip injection of glucose and blood glucose levels
760 were monitored with a glucometer for two hours to determine glucose tolerance (A). Unfasted
761 mice received an ip injection of insulin and blood glucose levels were monitored with a
762 glucometer for 2 hours to determine insulin sensitivity (B). The area under the curve (AUC) for
763 each assay are inset in pre-symptomatic (left) and symptomatic (right) cohorts. Fasting (C) and
764 fed (D) blood glucose levels were determined from t=0 during the GTT and ITT, respectively.

765 Data are represented as means ± SEM. *p<0.05 based on a two-way ANOVA with Sidak's post
766 hoc (A-D) and a two-tailed Welch's t test (n=9-16).

767 *Figure 4 – Liver glucose metabolism and plasma adipokines*. qRT-PCR was used to determine
768 hepatic relative gene expression profiles (A) of gluconeogenesis (G6PC, PEPCK), glycolysis
769 (GLUT2, GCK), and glycogenesis (GYS2). Circulating visfatin (B), adiponectin (C), and leptin
770 (D) determined by ELISA from plasma collected at the time of euthanasia. Data are represented
771 as means ± SEM. *p<0.05 based on a two-tailed Welch's t test (n=4-12). Abbreviations: G6PC -
772 glucose-6-phosphatase, PEPCK - phosphoenolpyruvate carboxykinase, Glut2 - glucose
773 transporter 2, GCK - glucokinase, GYS2 - glycogen synthase 2 (GYS2)

774 *Figure 5 – Senescent cell and inflammation markers in vWAT and SubQ.* qRT-PCR was used
775 to determine vWAT (A) and SubQ (B) relative gene expression profiles of senescence ($p16^{Ink4\alpha}$,
776 $p21^{Cip1}$) and inflammation (TNFα, IL-10, IL-6, MCP1). Data are represented as means ± SEM.
777 *p<0.05, **p<0.01, ***p<0.001, ****p<0.0001 based on a two-tailed Welch's t test (n=4-12).
778 Abbreviations: TNFα – tumor necrosis factor alpha, IL – interleukin, MCP1 – monocyte
779 chemoattractant protein 1.

780 Figure 6 - *Senescent cell and inflammation markers in the hippocampus.* qRT-PCR was used
781 to determine hippocampal relative gene expression profiles (A) of senescence ($p16^{Ink4\alpha}$, $p21^{Cip1}$),
782 inflammation (TNFα), and memory (AdipoR, LepR, Creb1, PRGN), while soluble $A\beta_{42}$ (B) was
783 determined by ELISA. Data are represented as means ± SEM. *p<0.05, **p<0.01 based on a
784 two-tailed Welch's t test (n=4-12). Abbreviations: TNFα – tumor necrosis factor alpha, AdipoR
785 – adiponectin receptor, LepR – leptin receptor, Creb1 – cyclic AMP Response Element-Binding
786 Protein 1, PRGN – progranulin.

787

Table 1: The number of mice in each cohort as well as the number of mice that experienced post-surgical mortality for that cohort.

| | Pre-Symptomatic $APP^{NL-F}$ | | | | Symptomatic $APP^{NL-F}$ | | | |
|---|---|---|---|---|---|---|---|---|
| Cohort | Male Sham | Male VFR | Female Sham | Female VFR | Male Sham | Male VFR | Female Sham | Female VFR |
| Mice | 10 | 20 | 15 | 17 | 25 | 9 | 14 | 15 |
| Mortality | 0 | 0 | 0 | 2 | 0 | 4 | 2 | 2 |

Table 2: A list of forward and reverse primers.

| Gene Name (Abbreviation) | Forward Primer | Reverse Primer |
|---|---|---|
| Acetyl-CoA Carboxylase (ACC) | 5'-ATGGGCGGAATGGTCTCTTTC-3' | 5'-TGGGGACCTTGTCTTCATCAT-3' |
| Adiponectin Receptor 1 (AdipoR1) | 5'-TCTTCGGGATGTTCTTCCTGG-3' | 5'-TTTGGAAAAAGTCCGAGAGACC-3' |
| Adipose Triglyceride Lipase (ATGL) | 5'-GGATGGCGGCATTTCAGACA-3' | 5'-CAAAGGGTTGGGTTGGTTCAG-3' |
| Beta-2 Microglobulin (BDM) | 5'-AAGTATACTCACGCCACCCA-3' | 5'-AGGACCAGTCCTTGCTGAAG-3' |
| Cyclic AMP Response Element-Binding Protein 1 (CREB1) | 5'-CCCAAAAACGAAGGGAAATCCT-3' | 5'-CCTGGTGCATCAGAAGATAAGTC-3' |
| Fatty Acid Elongase Enzyme 6 (Elovl6) | 5'-GAAAAGCAGTTCAACGAGAACG-3' | 5'-AGATGCCGACCACCAAAGATA-3' |
| Fatty Acid Synthase (FAS) | 5'-GGAGGTGGTGATAGCCGGTAT-3' | 5'-TGGGTAATCCATAGAGCCCAG-3' |
| Glucokinase (GLK) | 5'-TGAGCCGGATGCAGAAGGA-3' | 5'-GCAACATCTTTACACTGGCCT-3' |
| Glucose-6-Phosphatase (G6PC) | 5'-CGACTCGCTATCTCCAAGTGA-3' | 5'-GTTGAACCAGTCTCCGACCA-3' |
| Glucose Transporter 2 (GLUT2) | 5'-TCAGAAGACAAGATCACCGGA-3' | 5'-GCTGGTGTGACTGTAAGTGGG-3' |
| Glyceraldehyde-3-Phosphate Dehydrogenase (GAPDH) | 5'-AGGTCGGTGTGAACGGATTTG-3' | 5'-TGTAGACCATGTAGTTGAGGTCA-3' |
| Glycogen Synthase (GYS2) | 5'-ACCAAGGCCAAAACGACAG-3' | 5'-GGGCTCACATTGTTCTACTTGA-3' |
| Hormone Sensitive Lipase (HSL) | 5'-CCAGCCTGAGGGCTTACTG-3' | 5'-CTCCATTGACTGTGACATCTCG-3' |
| Interleukin-6 (IL-6) | 5'-CTGCAAGAGACTTCCATCCAG-3' | 5'-AGTGGTATAGACAGGTCTGTTGG-3' |
| Interleukin-10 (IL-10) | 5'-GCTCTTACTGACTGGCATGAG-3' | 5'-CGCAGCTCTAGGAGCATGTG-3' |
| Leptin Receptor (LEPR) | 5'-TGGTCCCAGCAGCTATGGT-3' | 5'-ACCCAGAGAAGTTAGCACTGT-3' |
| Monocyte Chemoattractant Protein-1 (MCP1) | 5'-CCACTCACCTGCTGCTACTCAT-3' | 5'-TGGTGATCCTCTTGTAGCTCTCC-3' |
| Monoglyceride Lipase (MGL) | 5'-CGGACTTCCAAGTTTTTGTCAGA-3' | 5'-GCAGCCACTAGGATGGAGATG-3' |
| $p16^{Ink4\alpha}$ | 5'-CGGTCGTACCCCGATTCAG-3' | 5'-GCACCGTAGTTGAGCAGAAGA-3' |
| $p21^{Cip1}$ | 5'-CCTGGTGATGTCCGACCTG-3' | 5'-CCATGAGCGCATCGCAATC-3' |
| Phosphoenolpyruvate Carboxykinase (PEPCK) | 5'-CTGCATAACGGTCTGGACTTC-3' | 5'-CAGCAACTGCCCGTACTCC-3' |
| Progranulin (PGRN) | 5'-ATGTGGGTCCTGATGAGCTG-3' | 5'-GCTCGTTATTCTAGGCCATGTG-3' |
| Protein Kinase A (PKA) | 5'-AGATCGTCCTGACCTTTGAGT-3' | 5'-GGCAAAACCGAAGTCTGTCAC-3' |
| Sterol Regulatory Element-Binding Protein 1 (SREBP1) | 5'-GATGTGCGAACTGGACACAG-3' | 5'-CATAGGGGGCGTCAAACAG-3' |
| Stearoyl-CoA Desaturase (SCD1) | 5'-TTCTTGCGATACACTCTGGTGC-3' | 5'-CGGGATTGAATGTTCTTGTCGT-3' |
| Tumor Necrosis Factor α (TNFα) | 5'-CAGGCGGTGCCTATGTCTC-3' | 5'-CGATCACCCCGAAGTTCAGTAG-3' |
| Ubiquitin Conjugating Enzyme E2 D2 (UBE2D2) | 5'-TGCCTGAGATTGCTCGGATCT-3' | 5'-TCGCATACTTCTGAGTCCATTCC-3' |

Figure 1

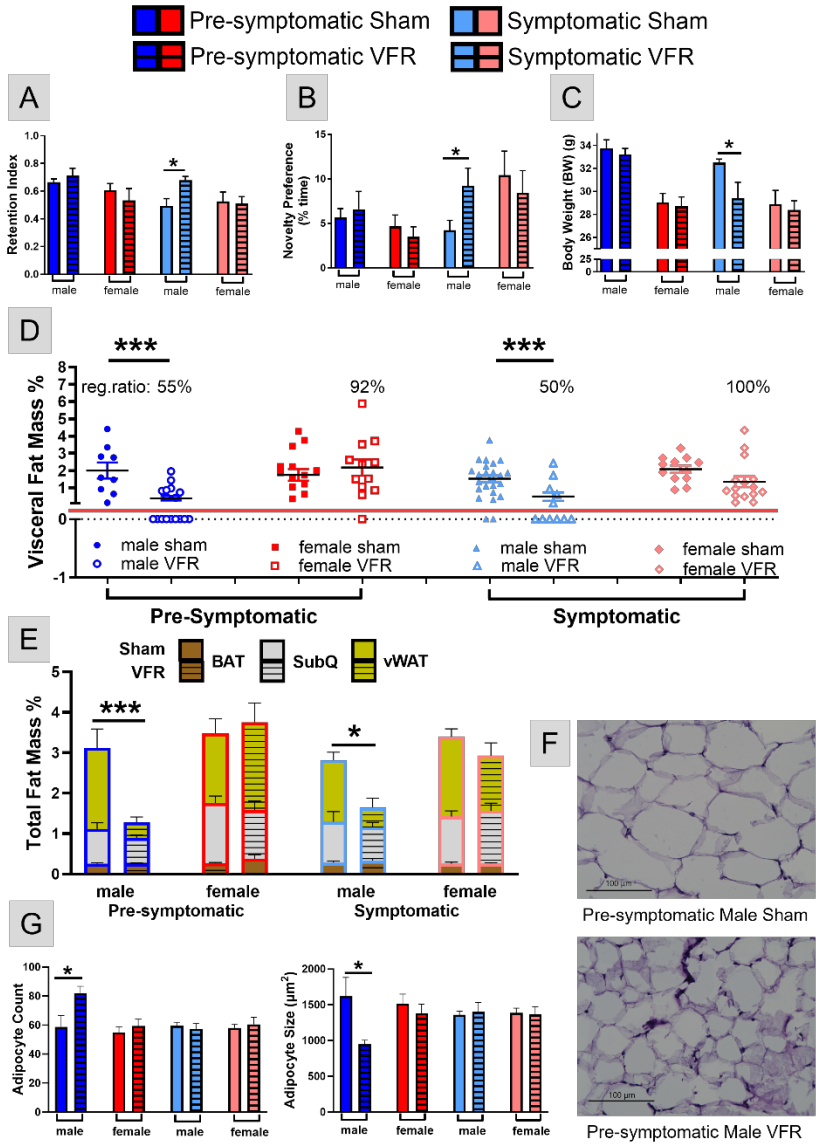
Pre-symptomatic Sham
Pre-symptomatic VFR
Symptomatic Sham
Symptomatic VFR
A
Retention Index
male
female
male
female
B
Novelty Preference (% time)
C
Body Weight (BW) (g)
D
Visceral Fat Mass %
reg.ratio: 55%
92%
50%
100%
male sham
male VFR
female sham
female VFR
Pre-Symptomatic
Symptomatic
E
Sham
VFR
BAT
SubQ
vWAT
Total Fat Mass %
Pre-symptomatic
Symptomatic
F
Pre-symptomatic Male Sham
Pre-symptomatic Male VFR
G
Adipocyte Count
Adipocyte Size (μm²)

Figure 2

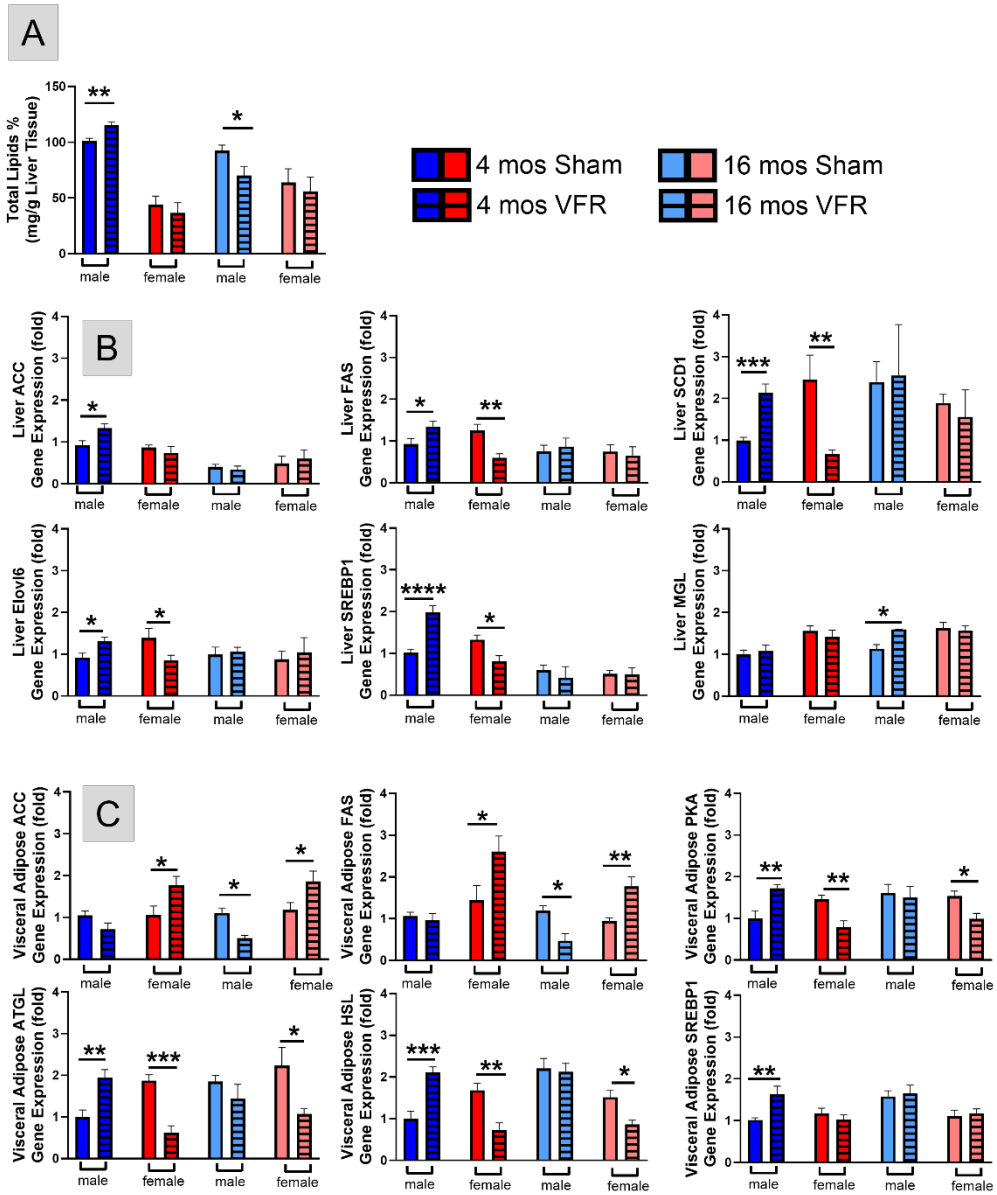
A
Total Lipids % (mg/g Liver Tissue)
4 mos Sham
4 mos VFR
16 mos Sham
16 mos VFR
B
Liver ACC Gene Expression (fold)
Liver FAS Gene Expression (fold)
Liver SCD1 Gene Expression (fold)
Liver Elovl6 Gene Expression (fold)
Liver SREBP1 Gene Expression (fold)
Liver MGL Gene Expression (fold)
C
Visceral Adipose ACC Gene Expression (fold)
Visceral Adipose FAS Gene Expression (fold)
Visceral Adipose PKA Gene Expression (fold)
Visceral Adipose ATGL Gene Expression (fold)
Visceral Adipose HSL Gene Expression (fold)
Visceral Adipose SREBP1 Gene Expression (fold)
male
female

Figure 3

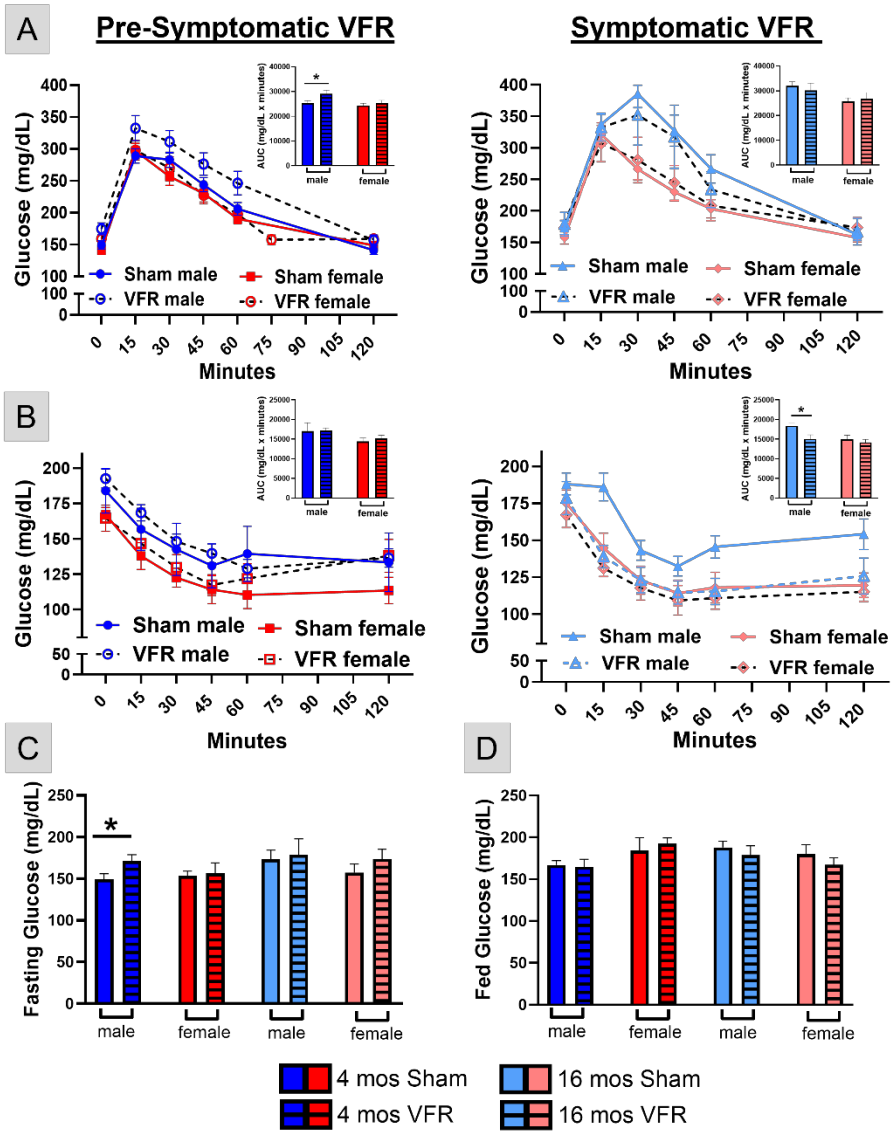
A
Pre-Symptomatic VFR
Symptomatic VFR
Glucose (mg/dL)
Minutes
Sham male
Sham female
VFR male
VFR female
AUC (mg/dL x minutes)
male
female
B
C
Fasting Glucose (mg/dL)
D
Fed Glucose (mg/dL)
4 mos Sham
4 mos VFR
16 mos Sham
16 mos VFR

Figure 4

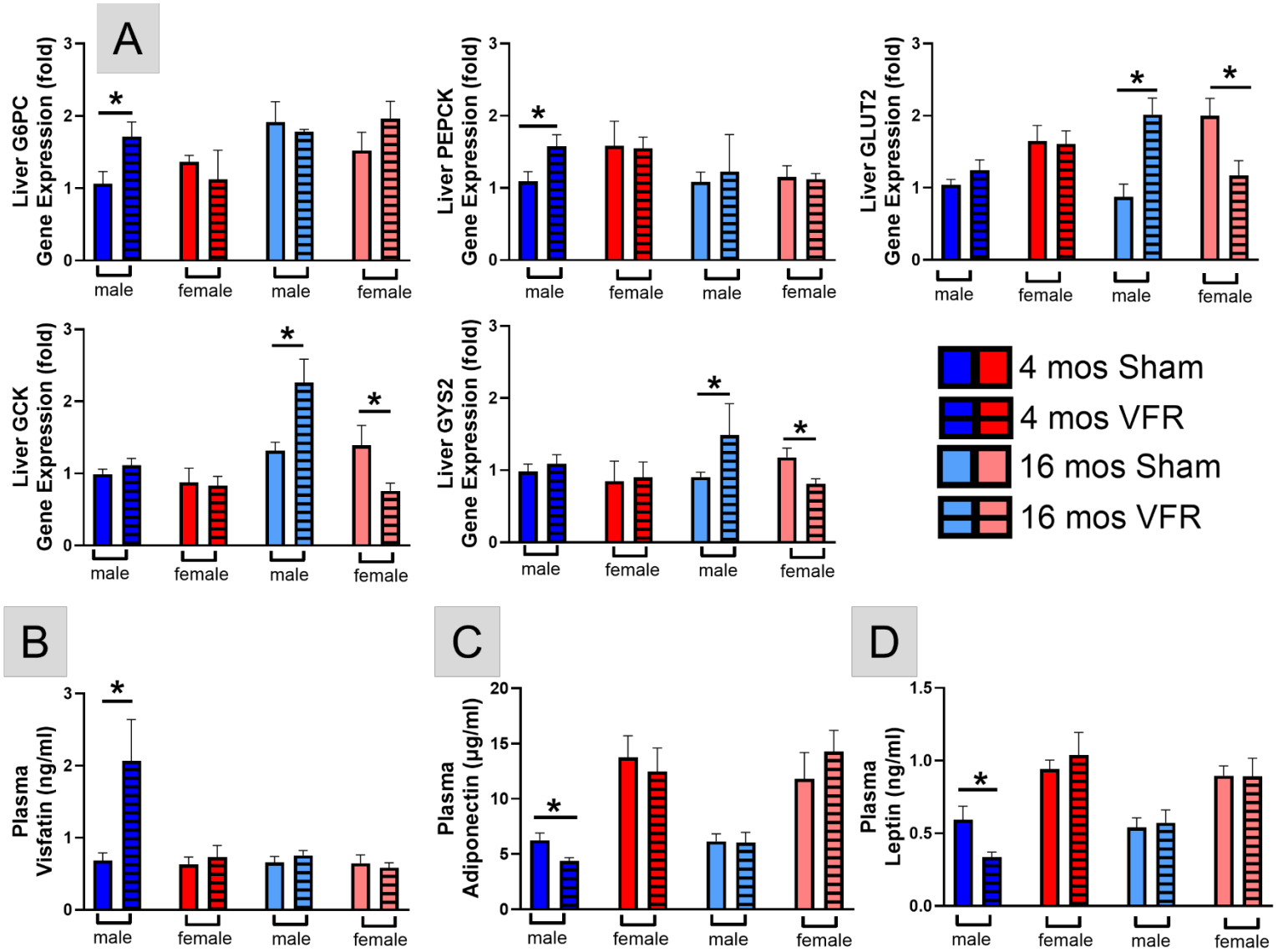
A
Liver G6PC Gene Expression (fold)
Liver PEPCK Gene Expression (fold)
Liver GLUT2 Gene Expression (fold)
Liver GCK Gene Expression (fold)
Liver GYS2 Gene Expression (fold)
male
female
4 mos Sham
4 mos VFR
16 mos Sham
16 mos VFR
B
Plasma Visfatin (ng/ml)
C
Plasma Adiponectin (µg/ml)
D
Plasma Leptin (ng/ml)

Figure 5

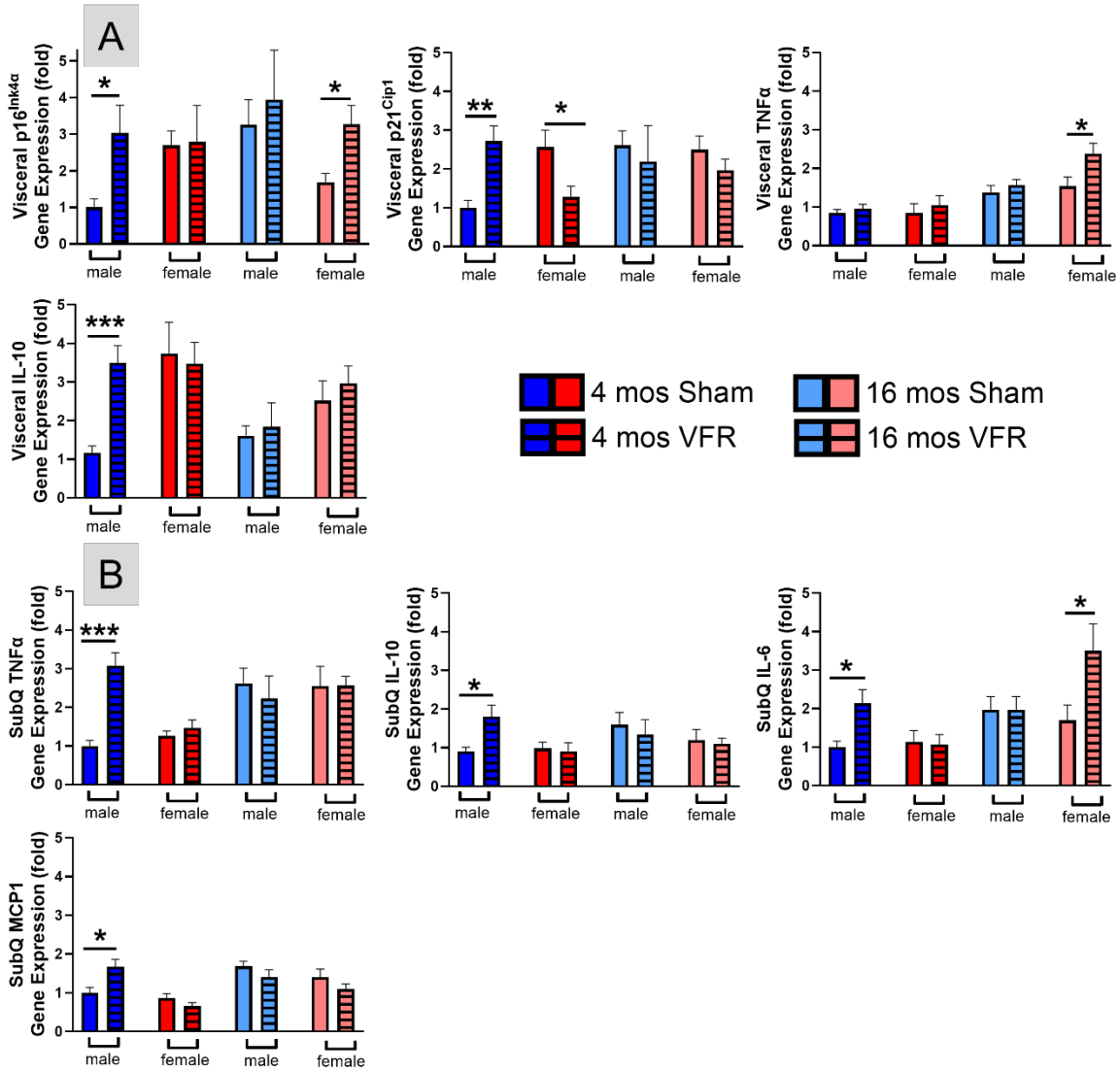
A
Visceral p16Ink4a Gene Expression (fold)
Visceral p21Cip1 Gene Expression (fold)
Visceral TNFα Gene Expression (fold)
Visceral IL-10 Gene Expression (fold)
4 mos Sham
4 mos VFR
16 mos Sham
16 mos VFR
B
SubQ TNFα Gene Expression (fold)
SubQ IL-10 Gene Expression (fold)
SubQ IL-6 Gene Expression (fold)
SubQ MCP1 Gene Expression (fold)
male
female

Figure 6

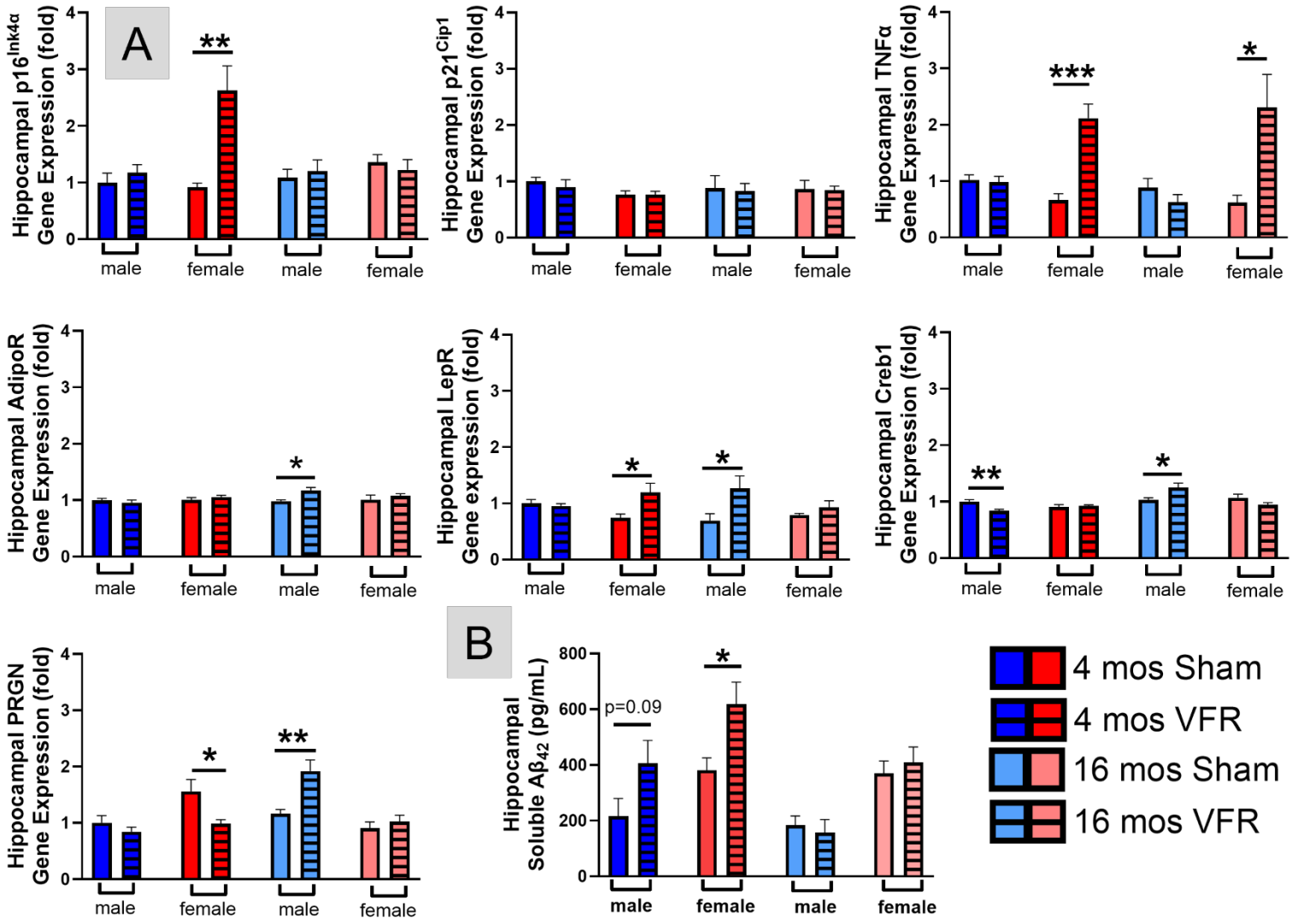
A
Hippocampal p16Ink4α Gene Expression (fold)
Hippocampal p21Cip1 Gene Expression (fold)
Hippocampal TNFα Gene Expression (fold)
Hippocampal AdipoR Gene Expression (fold)
Hippocampal LepR Gene expression (fold)
Hippocampal Creb1 Gene Expression (fold)
Hippocampal PRGN Gene Expression (fold)
B
Hippocampal Soluble Aβ42 (pg/mL)
p=0.09
male
female
4 mos Sham
4 mos VFR
16 mos Sham
16 mos VFR